

FILE COPY

ESD ACCESSION LIST

XNRI Call No. 83010

Copy No. 1 of 2 cys.

Technical Note

1975-36

Observations
of Synchronous Satellite ATS-3
with Three Coherent Radars

L. B. Spence
G. P. Banner

9 June 1975

Prepared for the Department of the Air Force
under Electronic Systems Division Contract F19628-73-C-0002 by

Lincoln Laboratory

MASSACHUSETTS INSTITUTE OF TECHNOLOGY

LEXINGTON, MASSACHUSETTS



Approved for public release; distribution unlimited.

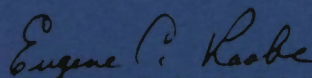
ADA013105

The work reported in this document was performed at Lincoln Laboratory, a center for research operated by Massachusetts Institute of Technology, with the support of the Department of the Air Force under Contract F19628-73-C-0002.

This report may be reproduced to satisfy needs of U. S. Government agencies.

This technical report has been reviewed and is approved for publication.

FOR THE COMMANDER



Eugene C. Raabe, Lt. Col., USAF
Chief, ESD Lincoln Laboratory Project Office

MASSACHUSETTS INSTITUTE OF TECHNOLOGY
LINCOLN LABORATORY

OBSERVATIONS OF SYNCHRONOUS SATELLITE ATS-3
WITH THREE COHERENT RADARS

L. B. SPENCE

G. P. BANNER

Group 96

TECHNICAL NOTE 1975-36

9 JUNE 1975

Approved for public release; distribution unlimited.

LEXINGTON

MASSACHUSETTS

ABSTRACT

A series of observations of NASA satellite ATS-3 have been made using coherent UHF, L-Band and X-Band radars, and detailed signatures of the satellite have been obtained. Coherent processing techniques were implemented that increased each radar's sensitivity by at least 40 dB over single pulse performance. A scattering model has been developed that agrees substantially with the measured signature.

I. INTRODUCTION

There have been a number of ways in which terrestrial radar has contributed to the development of space technology. Since the first artificial satellites were launched radar observations of satellites and attempts to interpret the observations in terms of satellite configuration and motion have been made.¹ With the increasing use of space, radar has contributed to the conceptually simple but important task of keeping track of orbiting objects of all sorts ranging from functioning satellites to pieces of debris associated with launches. Furthermore, on many occasions the need for radar diagnostics has occurred--a recent example being the question of the deployment of the solar panel on NASA's Skylab.

The Satellite Observables Program at Lincoln Laboratory has been directed toward extending such radar capabilities to very long distances--synchronous altitude and beyond. In particular, the program has sought to determine what features of distant artificial satellites are observable--and perhaps measureable--by ground-based instrumentation. To this end a number of satellites have been observed over the last few years using the Haystack Planetary Radar and the Millstone Hill Radar. More recently, the radar at the National Astronomy and Ionospheric Center² at Arecibo, Puerto Rico was used to further extend the data base. This paper draws on the observations that have been made on NASA satellite ATS-3 during the course of the program.

ATS-3 is a member of the NASA Applications Technology Satellite series. The satellite was launched into a synchronous equatorial orbit on 5 November 1967. It

1) G. H. Pettengill and L. G. Kraft, Jr., "Earth Satellite Observations Made with the Millstone Hill Radar," in Avionics Research: Satellites and Problems of Long Range Detection and Tracking, AGARDograph No. 40 (Pergamon Press, New York, 1960).

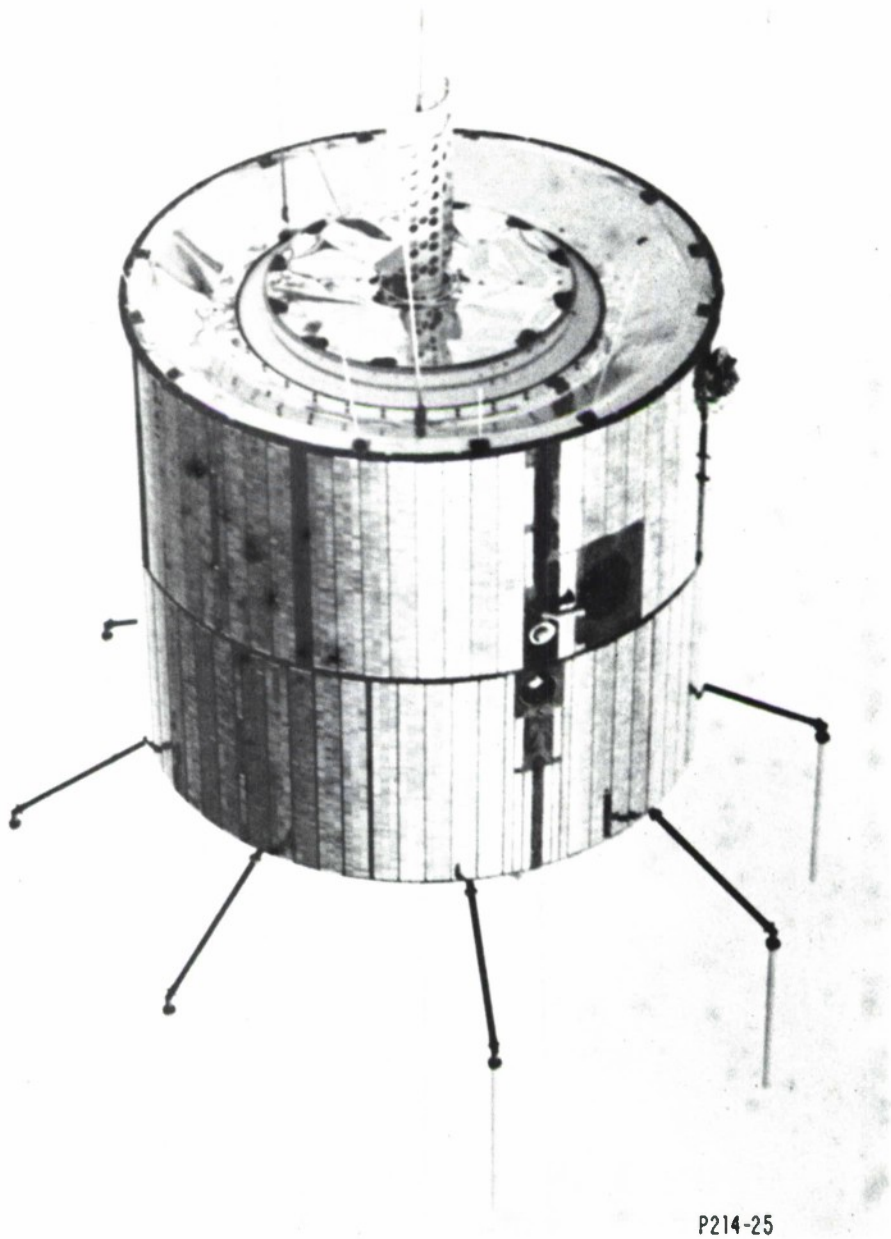
2) The National Astronomy and Ionospheric Center is operated by Cornell University under contract with the National Science Foundation.

carried a number of experiments to test candidate components and techniques for future communications, meteorological and navigation satellites. A photograph of the satellite is shown in Figure 1. From a radar observables viewpoint the major components of the satellite are the solar-cell covered body, the thin antennas attached to the top and bottom of the body cylinder and the parabolic cylindrical antenna on the top. The satellite spins about its axis of symmetry which is nominally perpendicular to the orbit plane. During the times of our observations, all scatterers spun with the satellite body. The spin period is about .62 second.

The radars used for the observations of ATS-3 were the Arecibo Planetary Radar (430 MHz, UHF), the Millstone Hill Radar (1295 MHz, L-Band) and the Haystack Planetary Radar (7840 MHz, X-Band). Relevant radar parameters are summarized in Table 1. These radars are distinguished from other available radars in several ways that serve to make them unique for synchronous altitude satellite observations. First, they are all high power radars with large antennas so they have enough power and aperture to observe targets at the range of interest. Second, they are coherent and by coherently processing the data further increases in sensitivity occur. Finally, they are pulsed so they can be turned off and on in the quarter second flight times or less typically encountered in these observations. This contrasts with other large radars like Goldstone which are essentially continuous with switching off and on in times on the order of the tens of minutes which are typical flight times to the planets and back.

An extensive data base exists on ATS-3. The times and duration of its observations by the three radars are summarized in Table 2. Over 14 hours of recorded data have been collected.

Important features of the recorded data can be inferred at once from estimates of the expected signal to noise ratio on the returned signal. While a detailed discussion of the scattering mechanisms will be given subsequently, it is sufficient to consider only the body cylinder return alone to roughly size the response. Table 3 shows the



P214-25

Fig. 1 ATS-3 shown suspended by cables prior to launch.

TABLE 1

OPERATING RADAR PARAMETERS DURING OBSERVATIONS

	<u>ARECIBO</u>	<u>MILLSTONE</u>	<u>HAYSTACK</u>
LOCATION	Arecibo, Puerto Rico (18.3° N, 66.8° W)	Westford, MA (42.6° N, 71.5° W)	Tyngsboro, MA (42.6° N, 71.5° W)
PEAK POWER	2.0 MW	3.0 MW	50 kW
PULSE LENGTH	500 μsec	500 μsec	2000 μsec
PRF	106.7 Hz	61.0 Hz	160 Hz
AVERAGE POWER	107 kW	91 kW	16 kW
WAVELENGTH	70 cm	23 cm	3.8 cm
ANTENNA GAIN	56 dB*	46.6 dB	66.1 dB
SYSTEM TEMPERATURE	430° K	150° K	150° K
SYSTEM LOSSES	2 dB	3.8 dB	1.0 dB
SINGLE PULSE S/N ON 1m ² TARGET AT 38, 500 km (36, 000 km FOR ARECIBO)	3.9 dB	-21.1 dB	-6.7 dB

*Measurements were taken at approximately 20° off zenith, where the one-way antenna gain is 4 dB below the 60 dB peak value at zenith.

TABLE 2
ATS-3 - RADAR DATA BASE

UHF (ARECIBO)		
<u>Date</u>	<u>Time (GMT)</u>	<u>Duration of Recorded Data</u> ¹
7 February 1974	0330	1475 sec
8 February 1974	0300-0800	5160 sec
12 February 1974	0500	2860 sec
13 February 1974	0400	<u>4840 sec</u>
		4.0 hr

L-BAND (MILLSTONE)		
<u>Date</u>	<u>Time (GMT)</u>	<u>Duration of Recorded Data</u>
3 April 1974	0000	1500 sec
7 June 1974	1100	1500 sec
18 July 1974	1000	2200 sec
19 July 1974	0500	<u>2400 sec</u>
		2.1 hr

X-BAND (HAYSTACK)		
<u>Date</u>	<u>Time (GMT)</u>	<u>Duration of Recorded Data</u>
4 June 1974	2000	910 sec
15 July 1974 ₂	0500	2275 sec
16 July 1974 ₂	*	*
18 July 1974	1000	2115 sec
19 July 1974	0500	2080 sec
3 October 1974	0830	600 sec
	1000-1300	3400 sec
		700 sec OP
5 October 1974	0000	500 sec
		500 sec OP
24-25 October 1974	2100	800 sec
		600 sec OP
	0200	1000 sec
		<u>600 sec OP</u>
		8.6 hr

1) All radars transmit RC and receive LC unless OP is noted which denotes transmit RC and receive RC.

2) The 16 July session ran from 1400 to about 1100 on the next day; runs were made every two or three hours. The total duration of recorded data was 14,890 sec.

expected extremes of cross-section variation over a typical day, assuming the cylinder is perfectly conducting. The variation is due to changes in satellite aspect angle, defined as the angle between the normal to the cylindrical surface and the radar line of sight. The range of aspect angles that occur over a typical day is also indicated. The actual variation of cross section with aspect angle will be discussed later.

Taking the maximum cross sections shown in the table and the per pulse signal-to-noise ratios on 1m^2 presented above, the following estimates result:

<u>Radar</u>	<u>Maximum S/N expected per pulse</u>
Arecibo	14 dB
Millstone	-18 dB
Haystack	-11 dB

Since it takes on the order of 10 dB S/N to have a readable signal, it follows that only at Arecibo would one expect to have enough signal to be able to analyze the received power versus time on a pulse by pulse basis. Such was in fact the case when the data were analyzed. A received power versus time record from 13 February 1974 at Arecibo is shown in Figure 2. Attempts to make similar plots for Millstone or Haystack show only noise as would be expected. The origin of the variations seen in the Arecibo signature is discussed below when a model is developed.

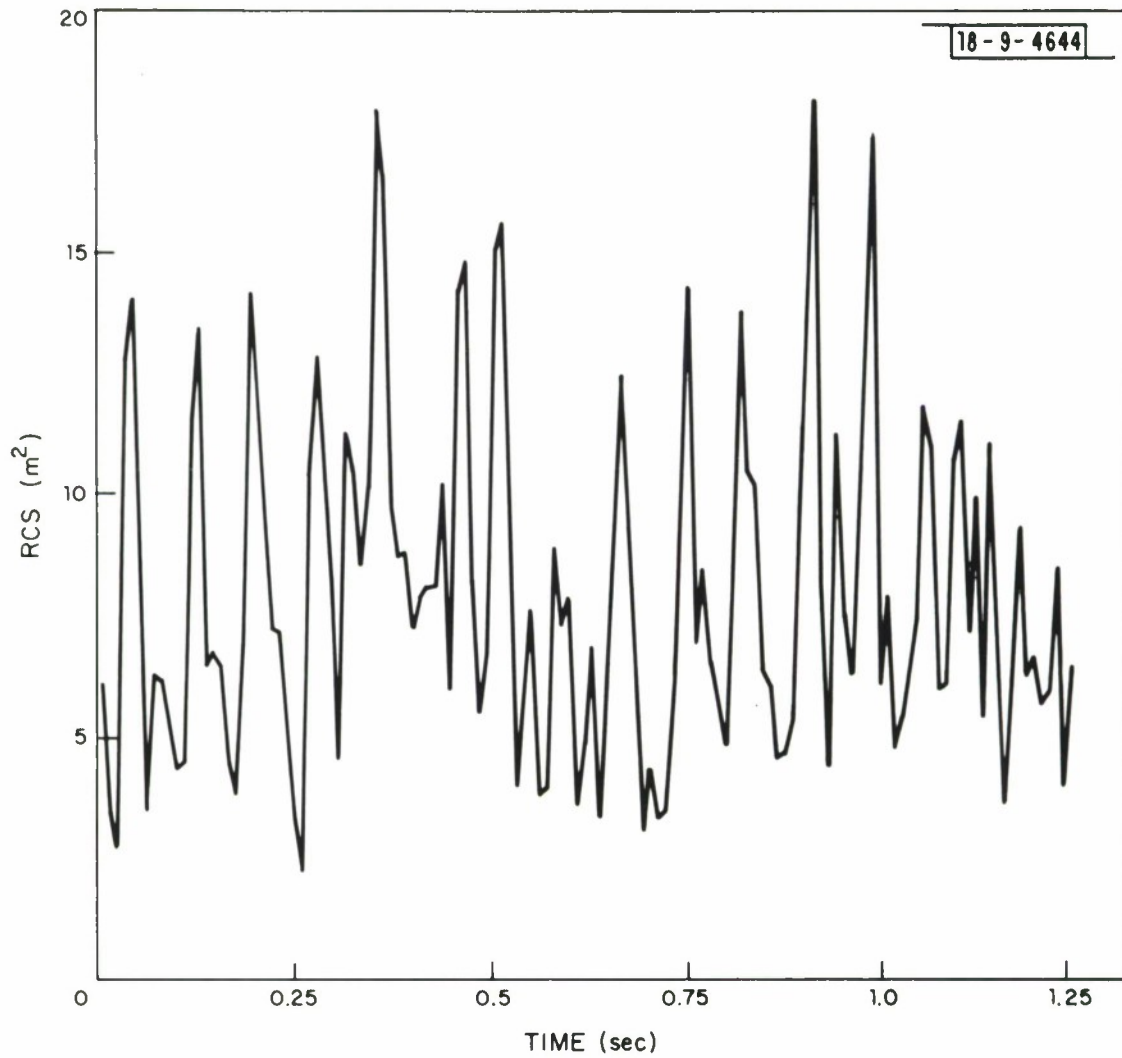


Fig. 2 Two cycles of ATS-3 signature at Arecibo;
(13 February 1974, 0417 GMT).

TABLE 3

EXPECTED CROSS SECTION VARIATION OF ATS-3 BODY CYLINDER

<u>Radar</u>	<u>Cylinder Aspect Angle</u>	<u>Range of σ</u>
ARECIBO (430 MHz)	$1.5^{\circ} - 4.5^{\circ}$	10 dBsm
MILLSTONE (1295 MHz)	$5.6^{\circ} - 7.4^{\circ}$	-5 dBsm to 3 dBsm
HAYSTACK (7840 MHz)	$5.6^{\circ} - 7.4^{\circ}$	Null to - 4 dBsm

II. COHERENT INTEGRATION

A time signature is not the only output from the radars. At all radars a stable local oscillator maintains phase coherence between successive pulses, so that the return from many pulses can be processed coherently. Such processing, known as coherent integration, can be implemented by passing the quadrature video output through a bank of digital filters each corresponding to a different doppler frequency shift. The Fast Fourier Transform (FFT) provides a very efficient means for implementing such a filter bank.

In practice the nominal B-Hz sampling bandwidth (=PRF) of the radar is divided by the FFT into a number of adjacent doppler bins equal to the number of pulses, M , that are processed, or integrated. Each of the M bins, which is B/M Hz wide, contains $1/M$ of the total noise energy in the quadrature video output. If the return signal from a satellite falls in a single bin, then the S/N in that bin is increased over the single-pulse S/N by the factor M , the reduction in noise energy.* In this manner, coherent integration increases the effective sensitivity of the radar.

To achieve the full gain in sensitivity associated with coherent integration, the received target signal must have components of width less than the width of a doppler bin. The width of the bin is inversely proportional to the integration time. The width of the received signal is a function of target motion, radar system stability and propagation path stability.

The general condition on target motion is that it be periodic (of which constant is a special case). Then, the target spectrum consists of narrow lines spaced at multiples of the periodic frequency. As will be discussed the energy from one of these lines can be made to fall into a single bin, provided the propagation path and radar system are stable.

*All the radars use matched filters whose bandwidths are greater than the sampling bandwidth. The noise in the matched filter bandwidth is folded into the sampling bandwidth. The matched filter bandwidth should be used in the radar equation. Then the gain achieved by coherent integration is correctly proportional to M .

With our method of implementing coherent integration, the limiting factor in the radar system has been found to be the step size of the local oscillator which produces real time corrections that effect the recorded doppler. Without the corrections the returned signal would not generally be in the receiver passband. However, the inverse of the minimum frequency detent dictates the time over which coherent processing can occur. The frequency detent and corresponding maximum coherent processing times are shown in Table 4 for the several radars we have used.

The principal contributor to propagation path stability is the ionosphere which introduces additional delay over free space propagation time due to the lower group velocity of the wave in the ionosphere. As the number of electrons in the ionosphere varies, changes in this delay occur which produce Doppler shifts on the returned radar signal. The magnitude of these Doppler shifts is shown to be¹

$$\Delta f = \frac{e^2}{\pi m c f} \frac{d}{dt} \int_0^R N dr$$

where e = charge on an electron (4.8×10^{-10} CGS units)

m = mass of an electron (9.1×10^{-28} gm)

c = velocity of light (3×10^{10} cm/sec)

f = radar frequency (Hz)

$\int_0^R N dr$ = Integrated electron content along propagation path.

If we assume typical values of integrated electron content in the ionosphere (5×10^{13} in a 1 cm^2 vertical column during the day, 5×10^{12} at night), we can calculate the Doppler shift that would be introduced by a possible Travelling Ionospheric Disturbance (TID) which could change the electron content by 2% over a 10 minute period. These results are shown in Table 5 for the three radars and the appropriate zenith angles during the observations of ATS-3 (20° at Arecibo, 50° at Millstone and Haystack). If these values were constant over a coherent integration interval, the only effect would be to shift the radar return signal by the amount indicated (1.1 bins

1) J. V. Evans and T. Hagfors, Radar Astronomy (McGraw Hill, New York, 1968), pg. 114.

TABLE 4

COHERENT INTEGRATION LIMITATIONS IMPOSED BY MINIMUM
DETENT IN LOCAL OSCILLATOR STEP

<u>RADAR</u>	<u>MINIMUM DETENT</u>	<u>MAXIMUM COHERENT INTEGRATION</u>
Arecibo	.01 Hz	100 sec
Millstone	.001 Hz	1000 sec
Haystack	.01 Hz	100 sec

TABLE 5

ESTIMATED DOPPLER SHIFTS INTRODUCED BY POSSIBLE
TID's DURING OBSERVATION OF ATS-3

	<u>DAYTIME</u>	<u>NIGHTTIME</u>
Arecibo (430 MHz) zenith angle - 20 ^o	.011	.0011
Millstone (1295 MHz) zenith angle - 50 ^o	.0054	.00054
Haystack (7840 MHz) zenith angle - 50 ^o	.00089	.000089

for a 100 second integration at Arecibo). Such a shift would therefore not limit the amount of coherent integration gain possible. Coherent integration would be degraded only when the Doppler shift would change resulting from a second time derivative of the electron density integral.

If we make the conservative assumption that the TID introduces an instantaneous Doppler shift of amount comparable to the values in Table 5, then only in the case of Millstone during the day is the shift significantly greater than the frequency detent the local oscillators cited in Table 4. Since most of our observations, particularly at Millstone have been made at night, it is not surprising as will be seen, we have been able to integrate at all frequencies to very close to the limits imposed by minimum frequency detent.

Before successful coherent integrations were possible, however, one more problem had to be overcome--mismatch between the true doppler of the target and the predicted doppler entered at the receiver. The problem is illustrated using Millstone data taken on Intelsat IV-F-7 on 10 April 1974. When a large number of pulses were processed with the FFT, the effect seen in Figure 3 was observed. The pictures in the graph correspond to the central 100 bins of three successive 8192-pulse FFT's. The total sampling bandwidth (=PRF) is 60.98 Hz, the width of each bin is therefore $60.98/8192 = 0.00744$ Hz and the total width of the 100 bins is 0.744 Hz. The three successive FFT's indicate that the peak signal return is sliding by about four bins for each integration.

The separation of four bins between the successive peaks suggests a constant rate of drift in the target doppler. Since ephemeris predictions were used to update pulse-by-pulse the doppler frequency in the receiver, it was postulated this drift in doppler relative to the ephemeris resulted from a mismatch between the true and the predicted satellite acceleration. With this in mind, adjustments were made to the phase of each pulse to compensate for the estimated value of the acceleration mismatch. By a recursive trial and error procedure, a best estimate of the mismatch was

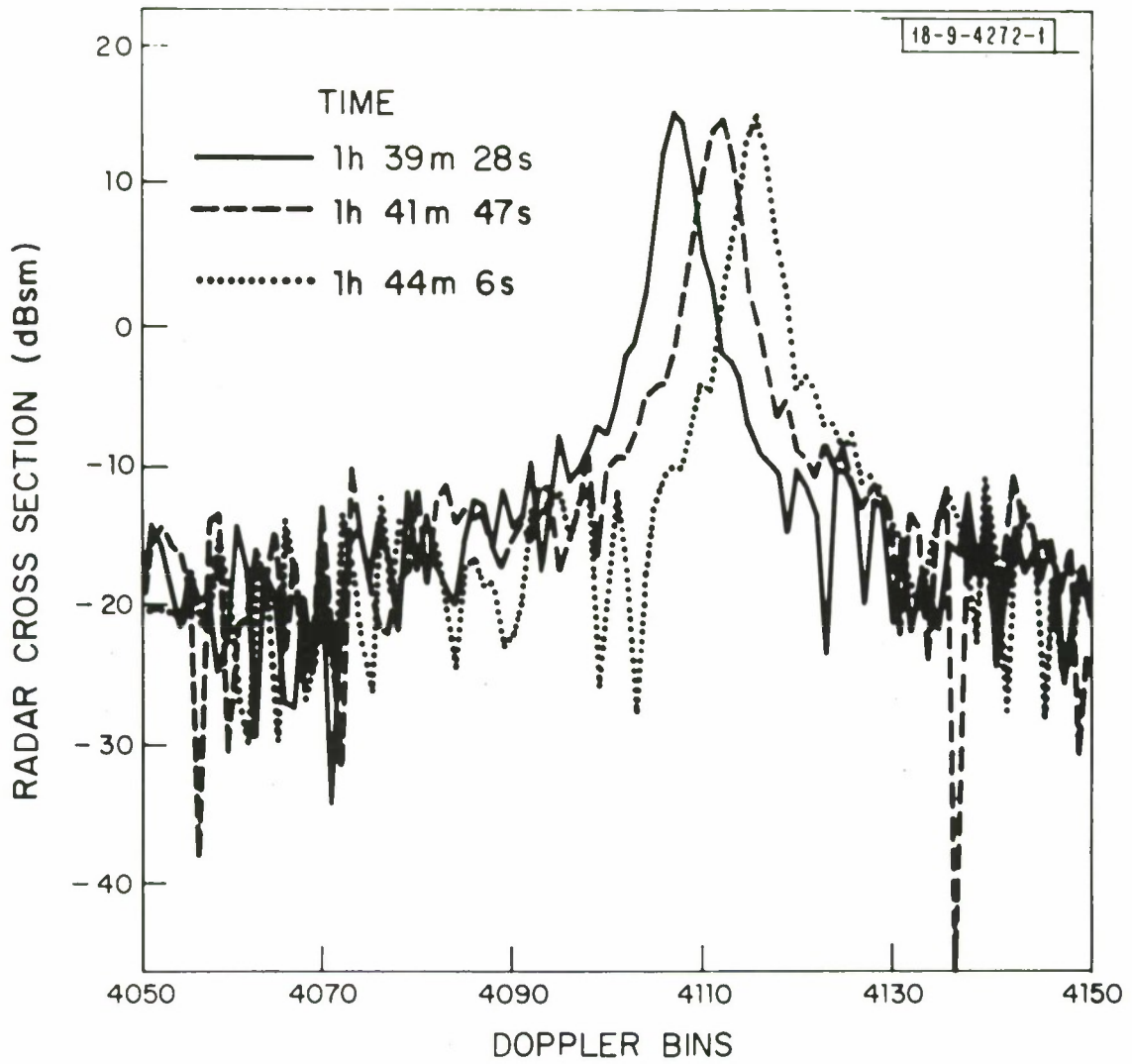


Fig. 3 Central 100 Doppler bins of three subsequent 8192-pulse integrations of Millstone data on Intelsat IVF-7.

determined to be $0.00002595 \text{ m/sec}^2$. This value corresponds to a constant drift in doppler of 0.0002242 Hz/sec , or a total shift of $.22 \text{ Hz}$ in a 1000 second interval. This shift is more than 2 orders of magnitude larger than might be expected from an ionospheric TID. Coherent processing up to $60,000$ pulses (984 seconds) was applied to the same data with and without the correction for the acceleration mismatch. Figure 4 indicates on a logarithmic (dB) scale the coherent gain achieved in both cases as well as the theoretical gain. The latter is directly proportional to the number of pulses integrated (or the integration time) and is 47.8 dB for $60,000$ pulses. The data points for the integration gains were obtained by measuring

$$\frac{S}{N} = \frac{(\text{integrated signal-to-noise ratio})}{(\text{average noise per bin})} = \frac{(\text{signal of peak FFT bin} - \text{average noise per bin})}{(\text{average noise per bin})}$$

and then dividing by the single-pulse signal-to-noise ratio, 0.93 , (-0.3 dB).

The figure indicates that while the maximum gain achieved by the uncorrected integration is 35.8 dB , the correction for the acceleration mismatch increases it to 47.3 dB . This result is only 0.5 dB below the theoretical limit.

The degradation in integration gain for the uncorrected case beyond 70 seconds is caused by the drift in doppler. A target return drifting at a constant rate $\gamma \text{ Hz/second}$ will spread over $\gamma T \text{ Hz}$ during a $T \text{ second}$ integration. Since the width of each doppler bin is $1/T$ the target signal will spread over γT^2 bins. Considering that coherent integration reduces the noise energy in each bin by a factor of T , when the target return begins to spread over more than 1 bin (that is, when $\gamma T^2 > 1$), the measured coherent gain will be proportional to

$$G \sim \frac{1/(\gamma T^2)}{1/T} \sim \frac{1}{T}$$

and will thus degrade by a factor of $1/T$. From the data in this case $\gamma T^2 = 1$ when $T = 66.8 \text{ seconds}$ and the coherent gain curve begins to degrade at this point as $1/T$.

Using the technique for performing corrected coherent integration, the ATS-3 data from Arecibo, Millstone, and Haystack have been processed. Plots

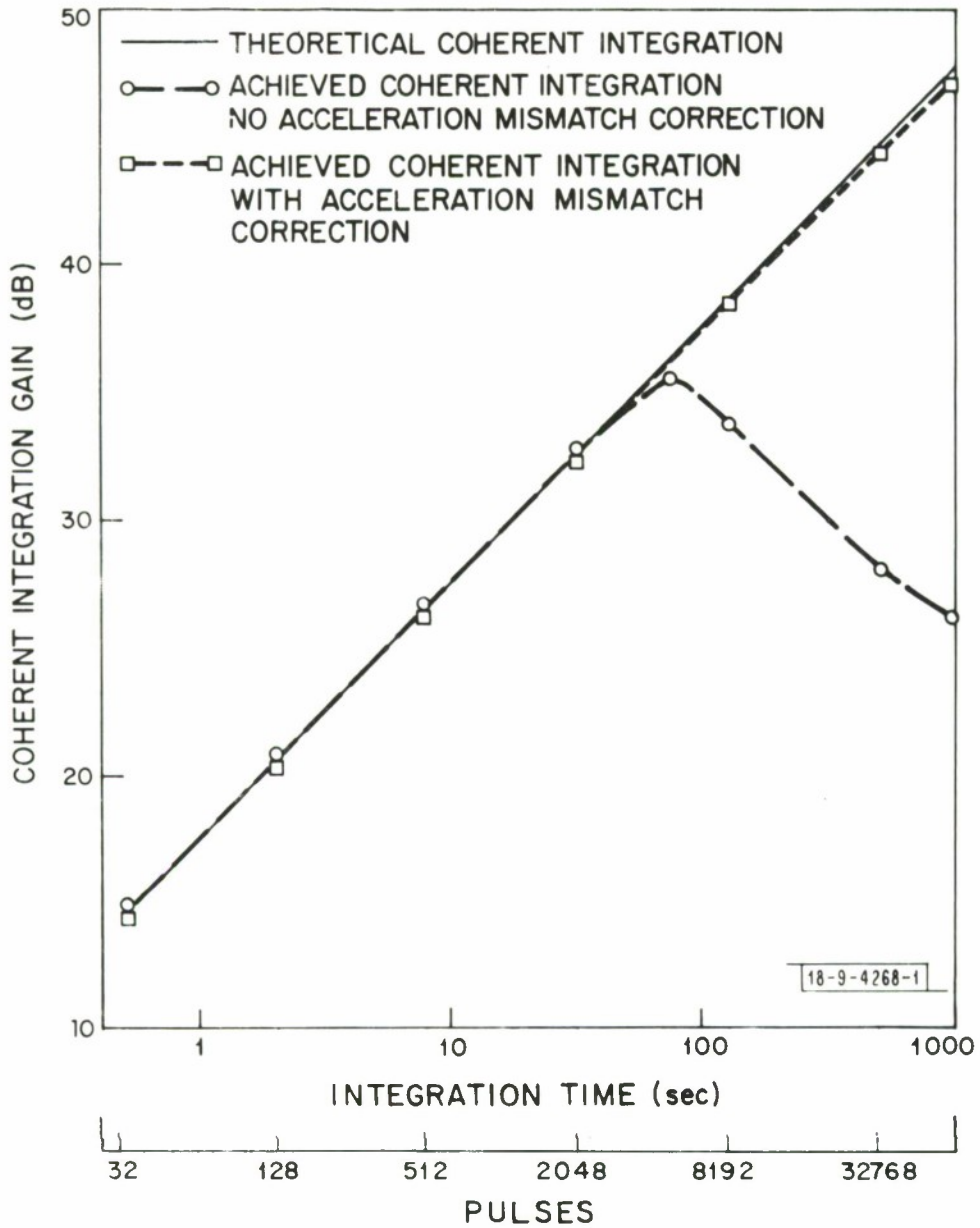


Fig. 4 Coherent integration gain versus integration time with Millstone Radar on Intelsat IVF-7, 10 April 1974.

corresponding to Figure 4 are shown in Figures 5 to 7. The achieved coherent gains and their impact on system sensitivity are summarized in Table 6.

Spectra resulting from long coherent integrations are shown in Figures 8 to 12. They represent the use of the best possible acceleration correction terms. The Arecibo (UHF) spectrum, Figure 8, is the strongest. It represents about 500 seconds of data; five 94 second coherent spectra were averaged incoherently to produce the result. The incoherent average was used to smooth out small variations from one coherent spectrum to the next. The major term is the zero frequency peak. Lines at multiples of eight times the satellite spin frequency (1.6 Hz) are next. Finally, there is "grass" consisting of lines spaced at the spin frequency. The noise level for this plot is at -42 dBsm which is offscale.

An example of a Millstone spectrum is shown in Figure 9. Only about 20% (or about 13 Hz) of the total spectrum of 60,000 points is shown. Graphing more lines reduces the clarity of the presentation. The portion shown contains the major information. Again, there is a strong line representing zero relative frequency accompanied by weaker lines spaced at integral multiples of the satellite spin frequency. In this case the "grass" is noise. The average noise is at about -20 dBsm. The remainder of the spectrum is mostly noise. There are, however, occasional lines at multiples of the spin frequency which are detectable although weak compared to the remainder of the spectrum.

The fact the Haystack wavelength is much less than the linear dimension of the major scatterers results in scattering lobe widths being sufficiently narrow that considerable variations of return with target aspect angle exist. Several representative spectra taken at Haystack at different times of day are shown in Figures 10 to 12. The aspect angles that were calculated for the observation times are also indicated. The chief characteristic of the spectra is the presence of many lines spaced at multiples of the spin frequency. Beyond this it has not been possible to be more definite about the presence of certain particular lines that are either always there or unusually

TABLE 6

RADAR SENSITIVITY USING COHERENT INTEGRATION

	<u>ARECIBO</u>	<u>MILLSTONE</u>	<u>HAYSTACK</u>
SINGLE-PULSE S/N ON 1 m^2 TARGET AT 38, 500 km (36, 000 km FOR ARECIBO)	3.9 dB	-21.1 dB	-6.7 dB
S/N USING 1 SECOND OF COHERENT INTEGRATION	24.2 dB	-3.3 dB	15.3 dB
MAXIMUM COHERENT INTE- GRATION INTERVAL	100 secs	1000 secs	100 secs
MAXIMUM ACHIEVED COHERENT INTEGRATION GAIN	40.0 dB	47.3 dB	41.7 dB
S/N USING MAXIMUM COHERENT INTEGRATION	43.9 dB	26.2 dB	35.0 dB

strong. Data runs made every few hours have proved insufficient to trace the evolution of the spectra with time. Still each spectrum is well defined and there is every indication that it is valid for the particular time.

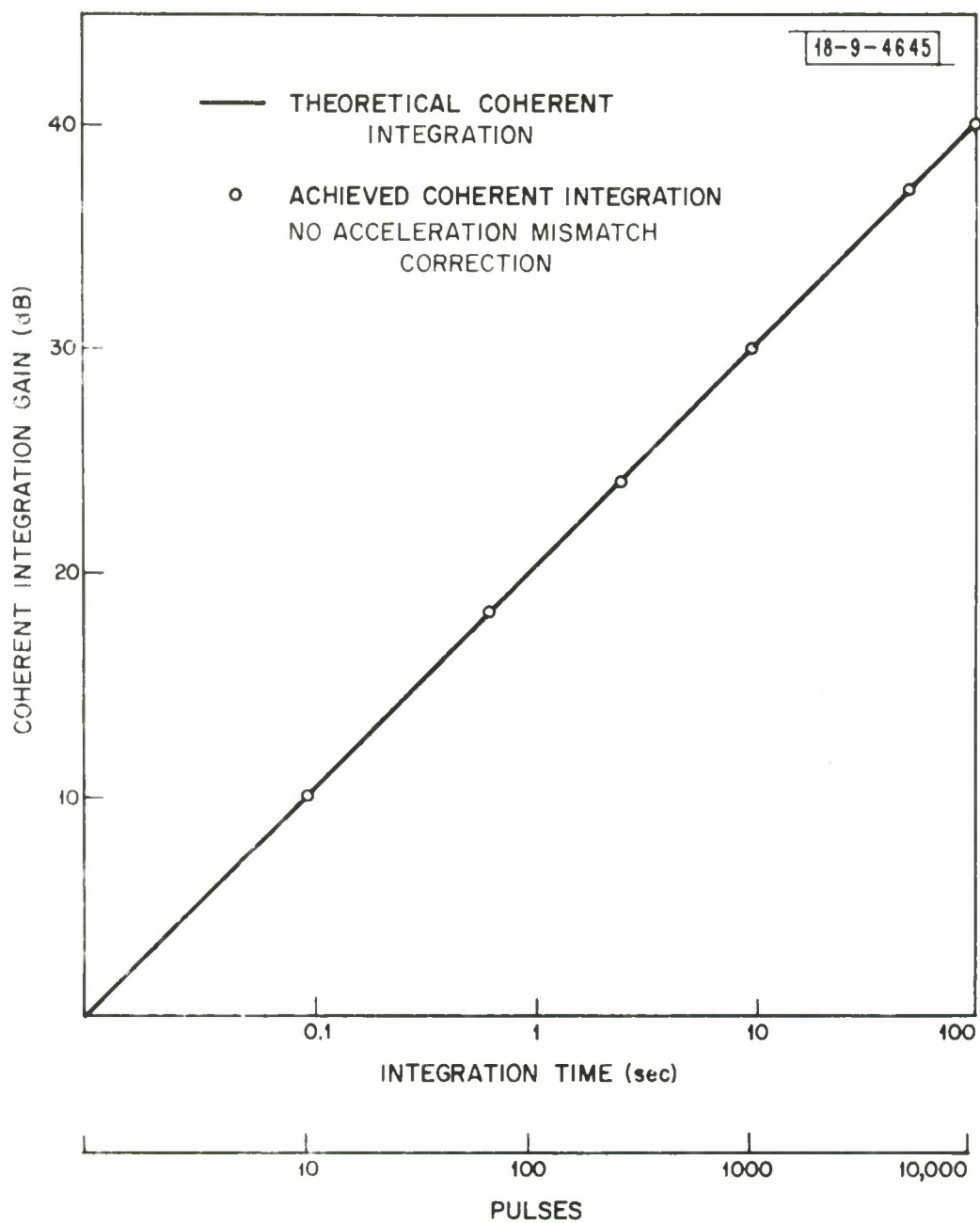


Fig. 5 Coherent integration gain versus integration time with Arecibo radar on ATS-3, 14 February 1974.

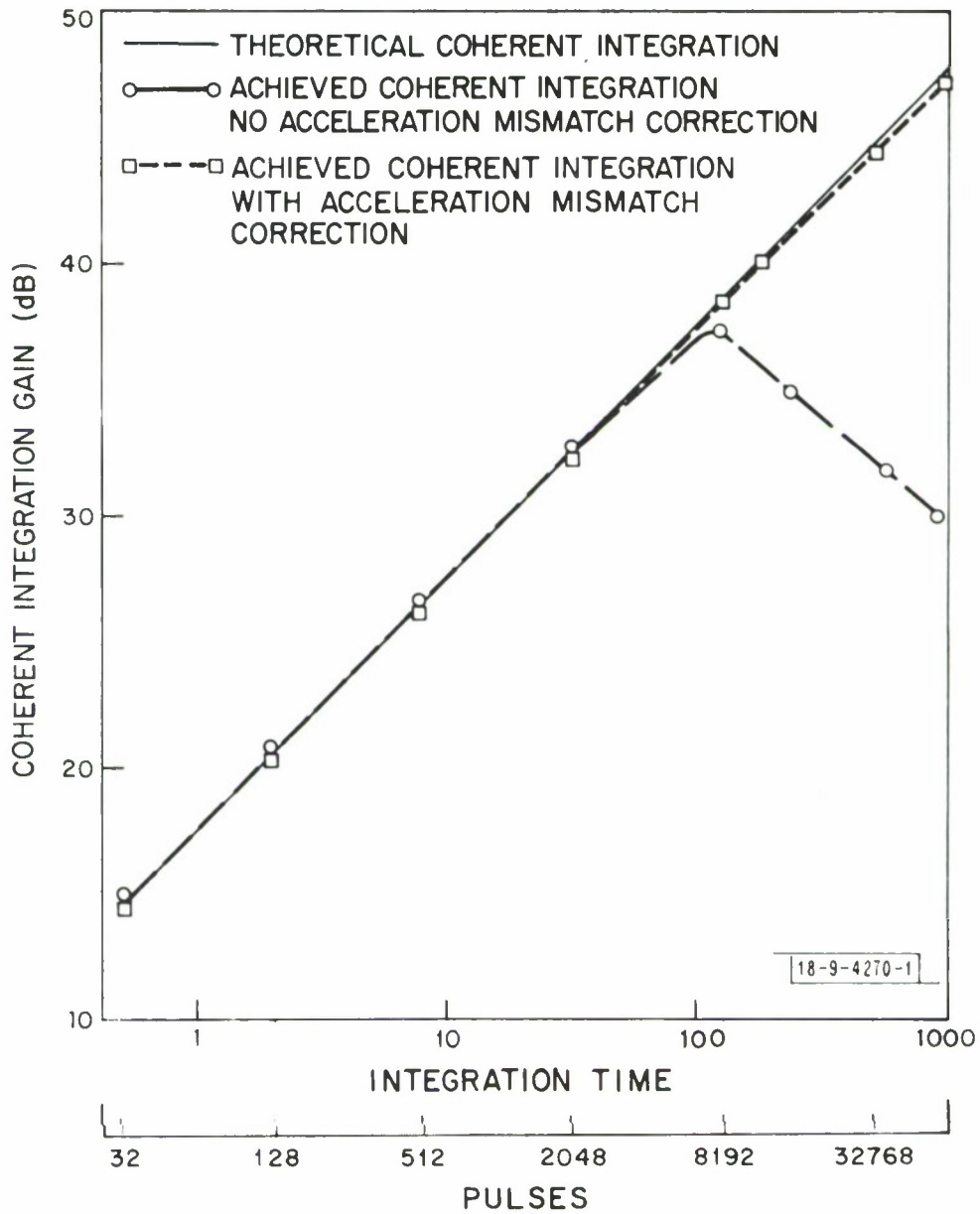


Fig. 6 Coherent integration gain vs. integration time with Haystack radar on ATS-3. 7 June 1974.

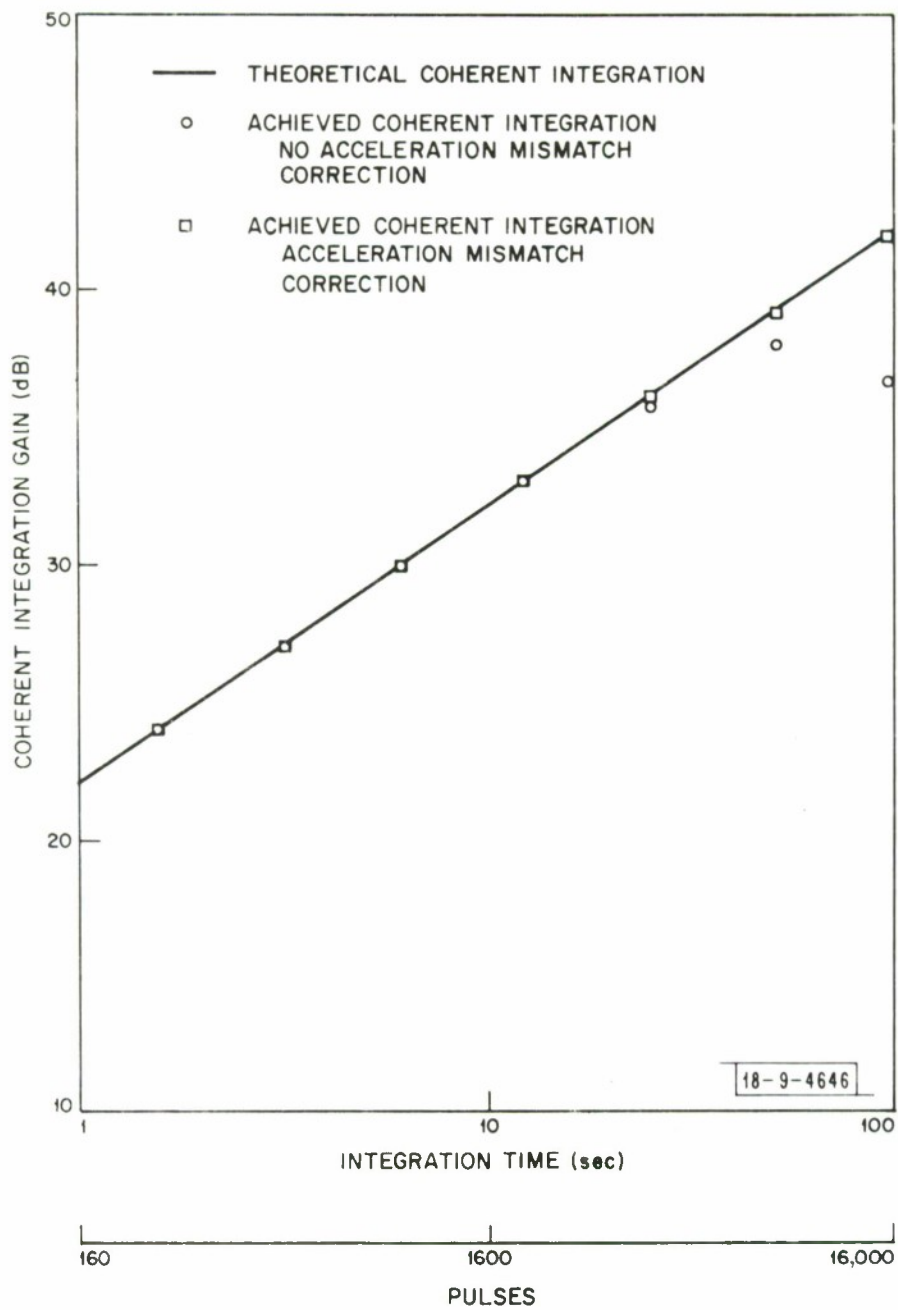


Fig. 7 Coherent integration gain vs. integration time with Haystack radar on ATS-3, 16 July 1974.

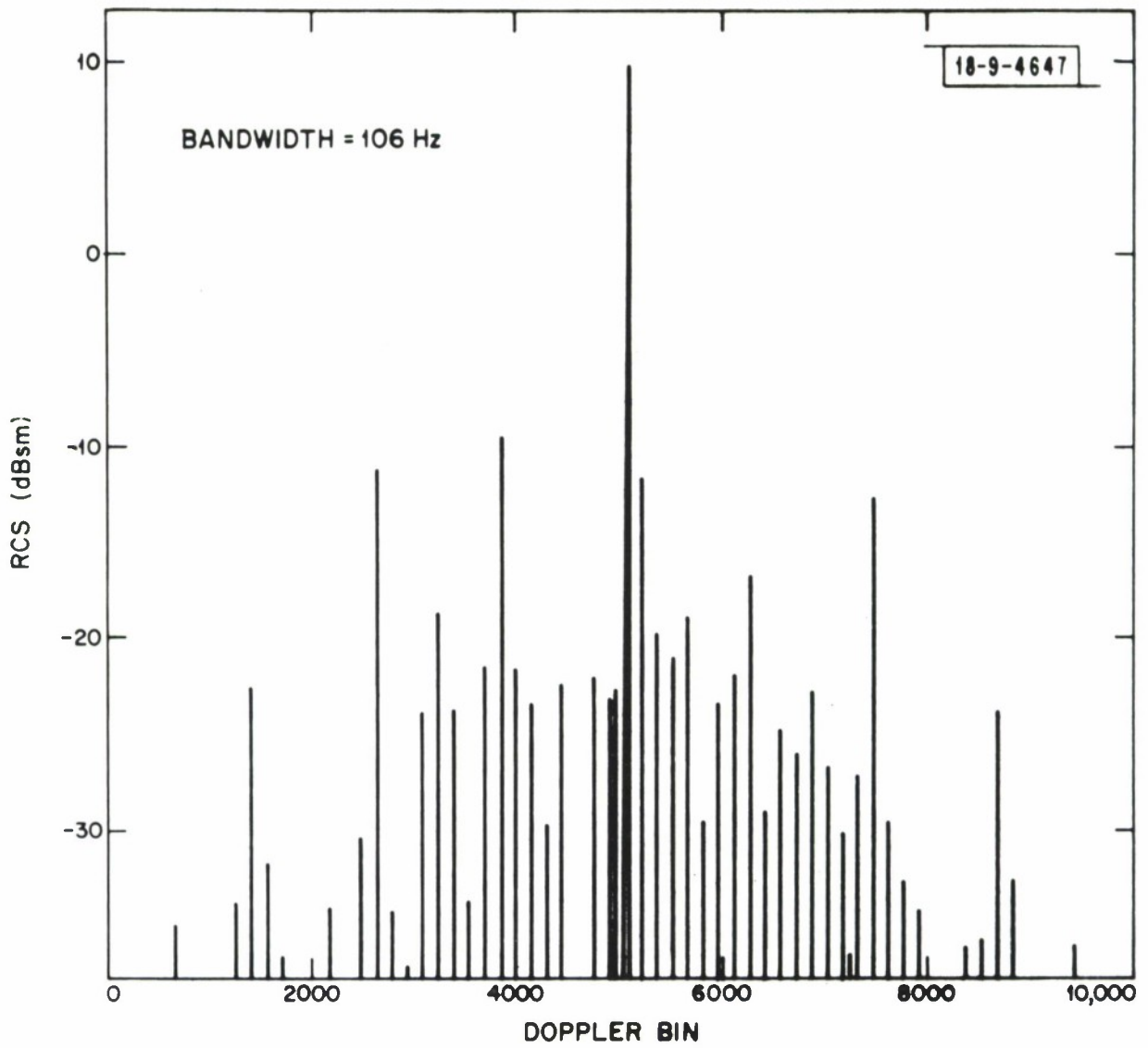


Fig. 8 Average of 5 10000 pulse (93.75 second) coherent integrations of ATS-3 data from Arecibo radar, 13 February 1974 .

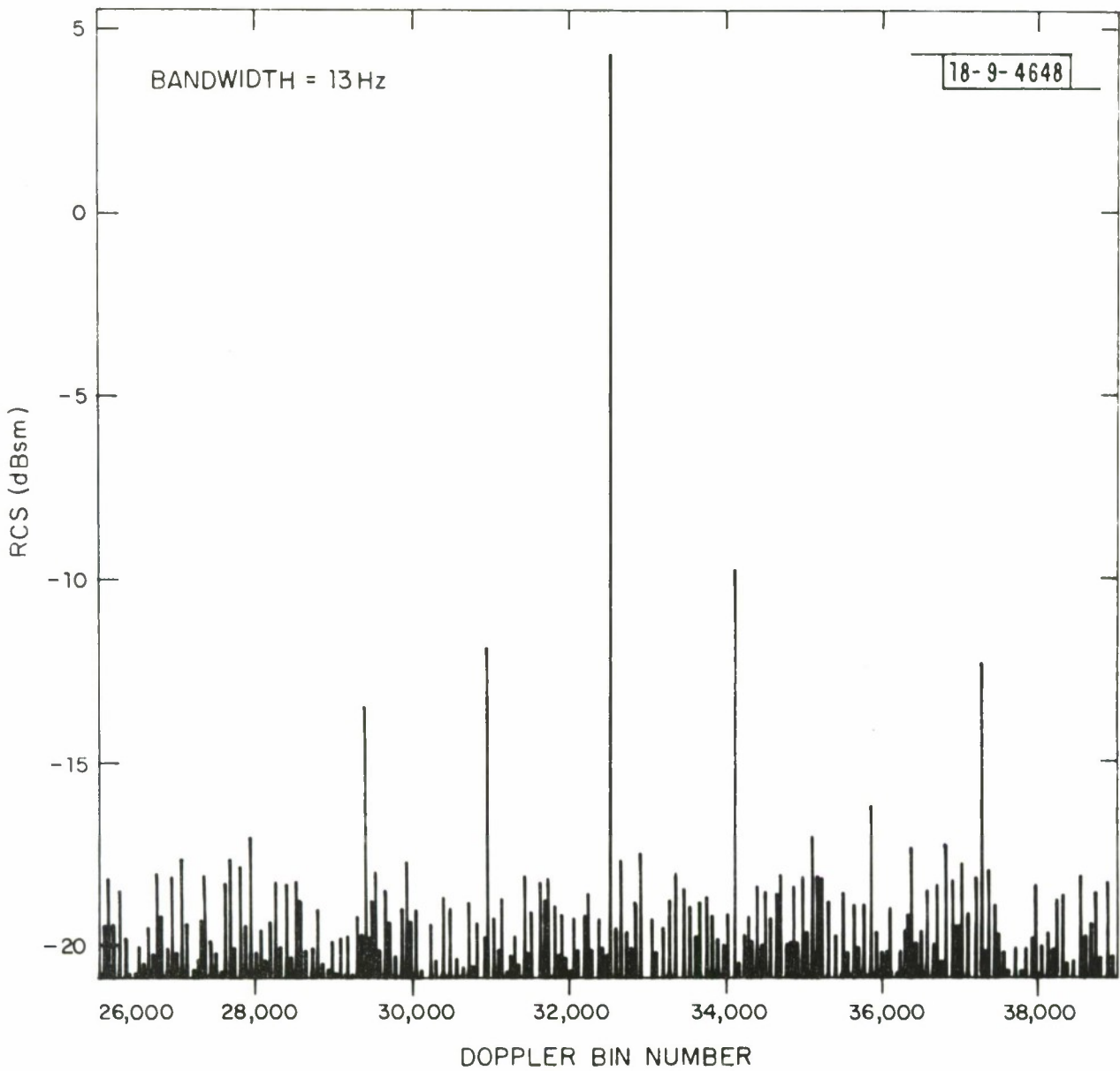


Fig. 9 13000 bins of a 60,000 pulse coherent integration of Millstone radar data on ATS-3, 7 June 1974.

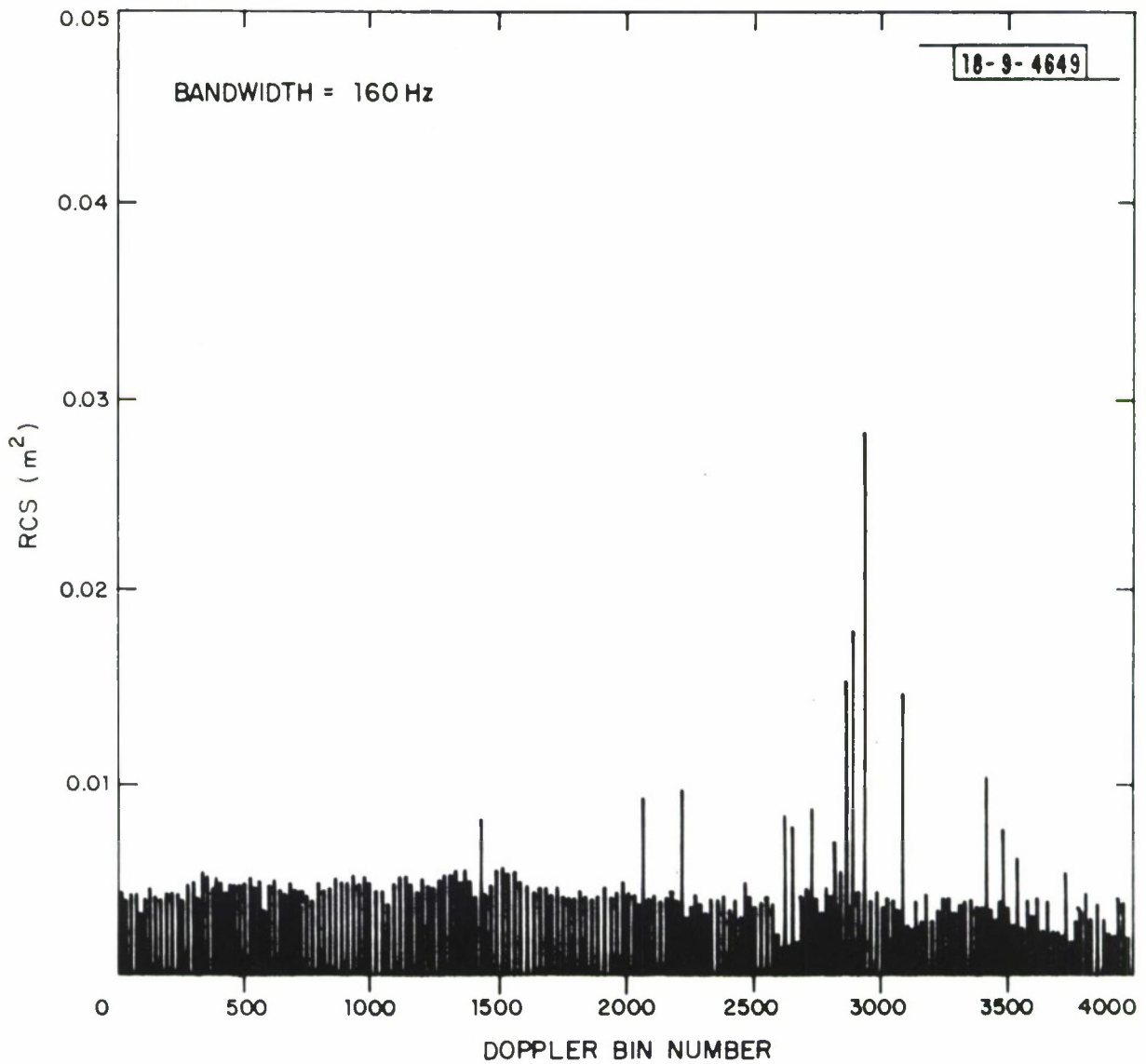


Fig. 10 Average of 28 4000 pulse (25 sec) coherent integrations of Haystack data on ATS-3, 1855 GMT, 16 July 1974. Calculated aspect angle is 5.8° .

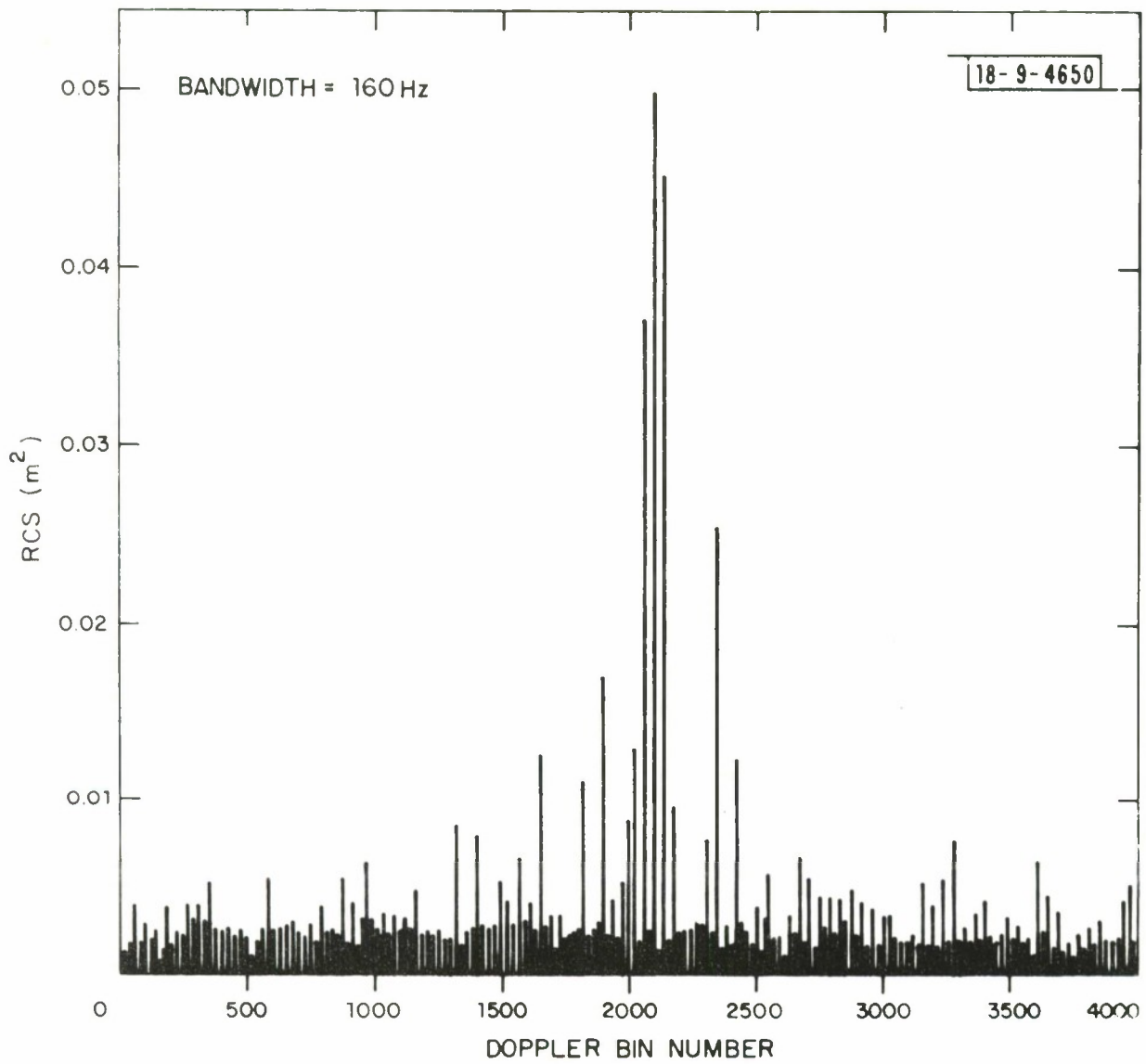


Fig. 11 Average of 19 4000 pulse (25 sec) coherent integrations of Haystack data on ATS-3, 1408 GMT, 16 July 1974. Calculated aspect angle is 6.8° .

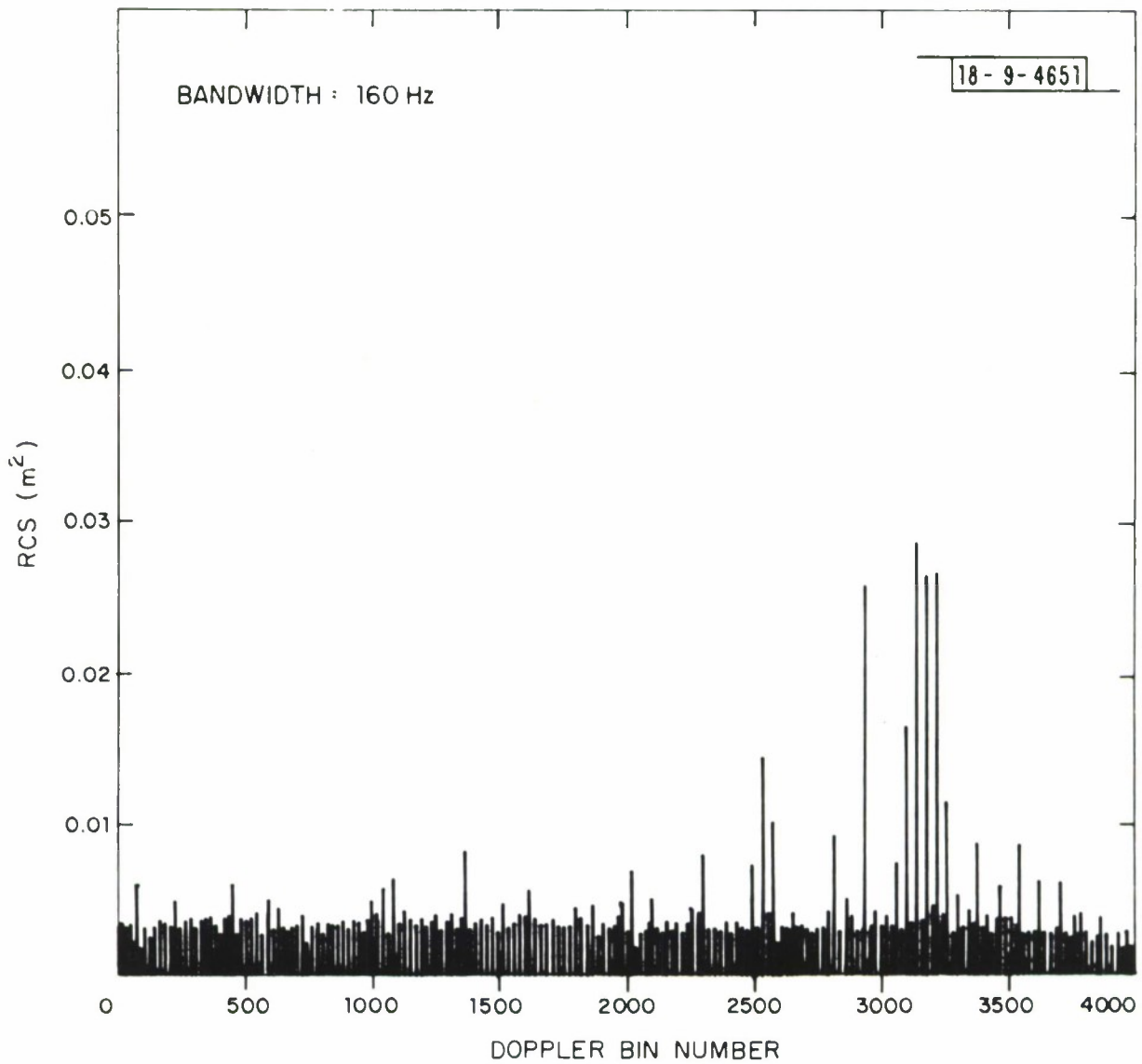


Fig. 12 Average of 40 4000 pulse (25 sec) coherent integrations of Haystack data on ATIS-3, 1043 GMT, 16 July 1974. Calculated aspect angle is 7.3° .

III. SCATTERING MODELS

Every external feature of the satellite body is a potential contributor to the observed cross-section. Indeed, even internal pieces connected to the surface by transmission lines of any sort need by considered. We initially examined the ATS-3 structure in order to identify the major scatterer and reduced the list of potential scatterers to those shown on Figure 13 along with relevant dimensions of the satellite. Models for each scatterer on this list were then developed and the models combined with known behavior of the satellite in an attempt to simulate the observed data.

The models that were used for the scatterers are shown in Figure 14. Of all the scatterers the parabolic antenna on the top is clearly the most complex. It consists of a number of interacting elements some of which like the perforated plates on the back are very difficult to model. The model that was used, flat plates for the front and rear, was taken as a first cut but proved to be acceptable. The body cylinder was taken as a perfectly conducting cylinder. Experience with other satellites suggested this to be a good approximation for solar panel covered spacecraft. In the case of the thin antennas on the top and bottom, two considerations were necessary. First, that they were bent structures and second that they had electrical terminations inside the satellite. In the case of the top antennas they were end-fed. The bottom communication antennas were quarter wave stubs at the end of the spider-like legs, making for a bent structure fed near the center as the overall scatterer. It was assumed that all the scatterers were electromagnetically independent.

The dynamic motion of the satellite in orbit is relatively simple. The satellite spins about an axis aligned with the body cylinder symmetry axis. The spin period is about 0.62 second. Over the course of a day the movement of the satellite in sub-orbital latitude ($+4^{\circ}$) is sufficient to change the aspect angle between the line of sight and the normal to the spin axis as shown for the several sites in Figure 15.

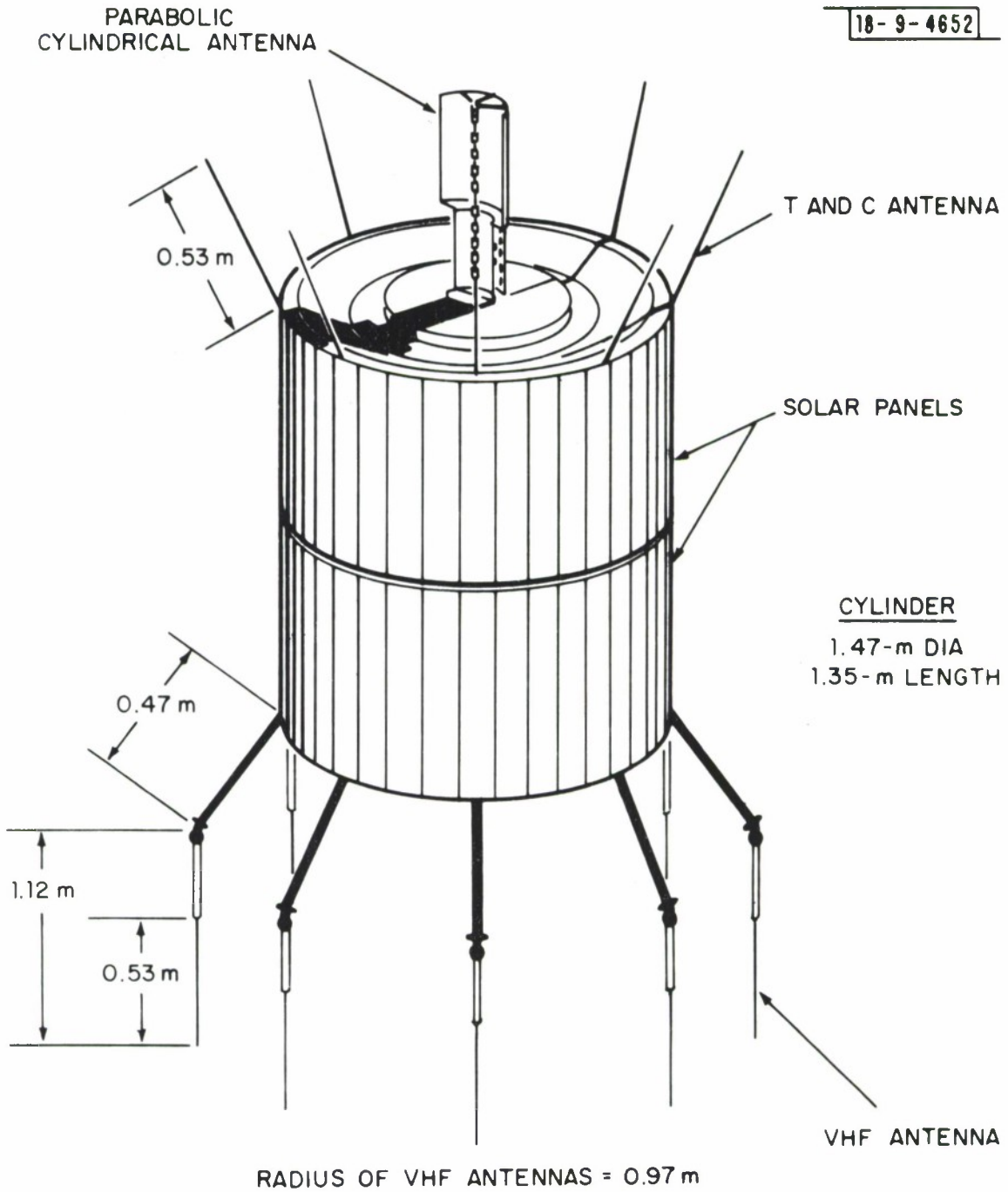


Fig. 13 ATS-3 dimensions and identification of potential scatterers.

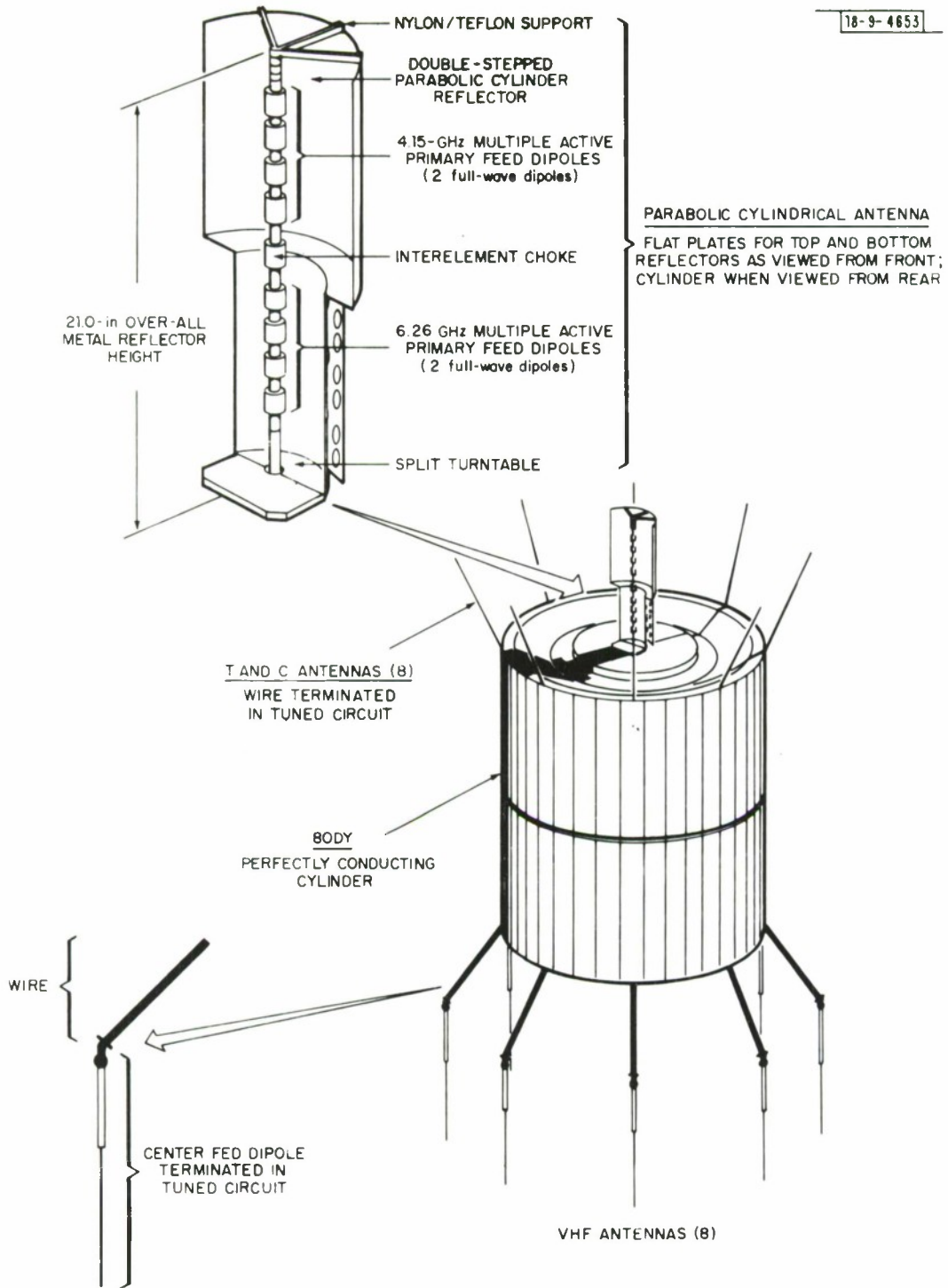


Fig. 14 Models for major scatters.

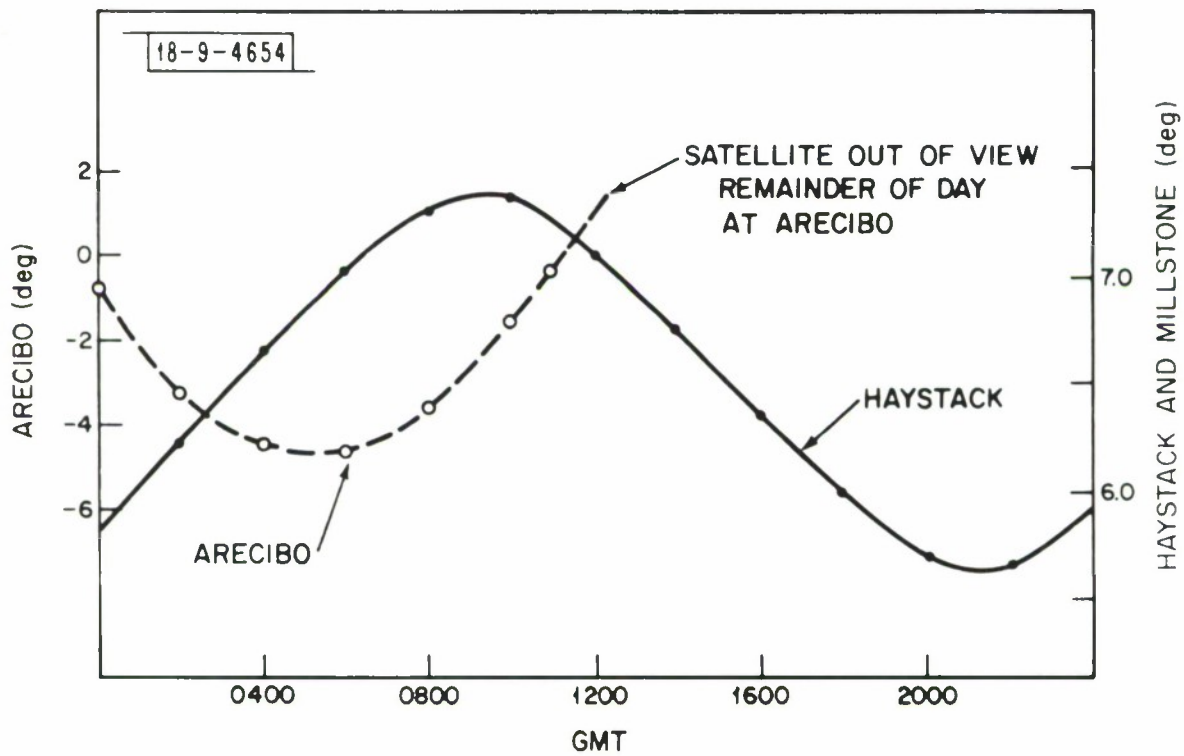


Fig. 15 Typical variation of satellite aspect angle during day from Haystack (July 16, 1974) and Arecibo (February 21, 1974).

A capability was developed which summed the amplitude and phase of the individual scatterers at subsequent points in the spin cycle to produce simulated radar signature of the target. Outputs were simulated time and frequency signatures for each radar frequency. In the following, results for each radar frequency are given.

A. Arecibo

The perfectly conducting cylinder model leads to an estimate of 10 dBsm for the body cylinder. The first null of the cylinder is at an aspect angle of about 15° so there is negligible variation of cross section over the 2 and 4° range of aspect angles which prevailed during the observations.

The T&C antennas on the top of the spacecraft were modeled by a set of straight wires making an angle of 20° with the vertical. While they are fed at their base for 140 MHz T&C use, the body cylinder does not appear to influence them so boundary conditions require a current null at the base. Thus, one would not expect the net impedance of the transmission line and load to have any effect regardless of its value. Consequently, each wire was modeled as a tilted unloaded wire independent of the rest.

The parabolic antenna presented problems as mentioned above. The model that was selected for UHF was as follows: The front of the antenna was taken as a flat plate with the projected area of the parabolic antenna. The presence of the feed and the offsets and curvature of the surface are all within a tenth of a wavelength straight on so interference effects are not expected to be large. Furthermore, the feed is essentially a wire that gives a calculated cross section 10 dB below the cross section calculated for the plates thereby mitigating still more the possibilities for interference. The lobe of the antenna is assumed to taper smoothly to the point where the antenna is viewed from the side. This assumption is justified by the observation that a plate the size of the antenna has essentially one lobe on each side. When the antenna is viewed from the side it is treated as a wire. In the back of the antenna as

can be seen on Figure 1 there are two flat perforated plates. The perforations were ignored in the calculation. In fact, the lobes of the plates are wide enough that they essentially constitute one plate and one lobe as seen by a UHF radar. The phase was accounted for using the distances from the satellite spin axis to the centers of the relevant scatterers.

The major question faced with the spider-leg like VHF antennas on the bottom of satellite was how to treat the loading. In lieu of specific information on the loads the following procedure was employed. First, the bent wire scattering patterns were calculated ignoring the effects of the load. Then, the results were used in the simulation program and that output compared with the measured data. As it turned out, the results compared well as will subsequently be discussed. Since loading can significantly reduce the cross section but not significantly increase it over that of an unloaded wire, it was shown to be negligible. One could have researched the loads and proceeded to solve the problem rigorously. Since, however, this technology of spacecraft antennas is one seldom encountered in new designs, the time necessary for such an investigation did not seem justified.

The above models were combined to produce a simulated signature of the satellite. The resultant time and spectral plots are shown in Figures 16 and 17. In all cases the lobes of the scattering pattern in the satellite spin axis-observation point plane were sufficiently broad that no noticeable variation with aspect angle occurred for the aspect angle range encountered at Arecibo.

The major variations between the actual and simulated time plots are related to data processing constraints. Since the actual signature is noisy, it is necessary to average a number of cycles (ten in this case) to get a good representation. Consequently, the variation of amplitude is reduced as corresponding peaks and nulls do not line up exactly over the averaging interval. Second, since the samples are taken at discrete points there is the problem of getting the true values for peaks and nulls. This problem manifests itself in the present case in a reversal of null depths between

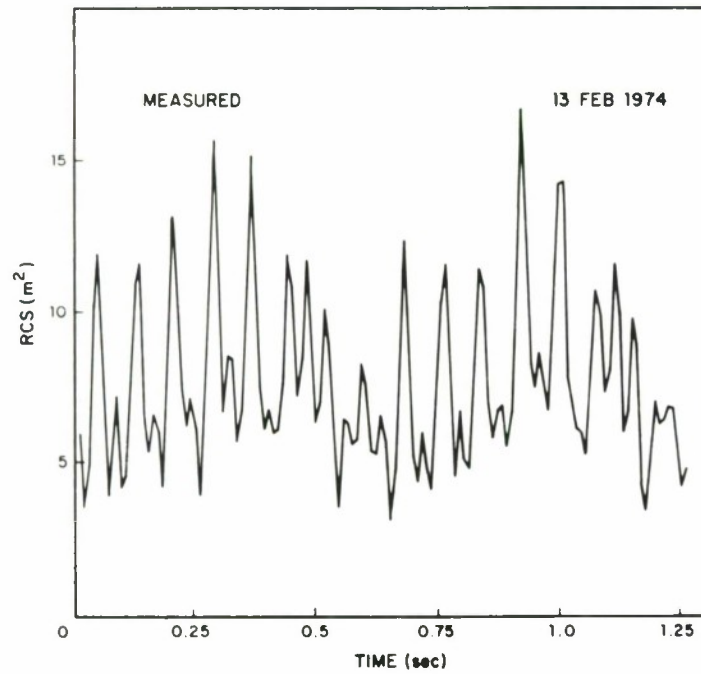
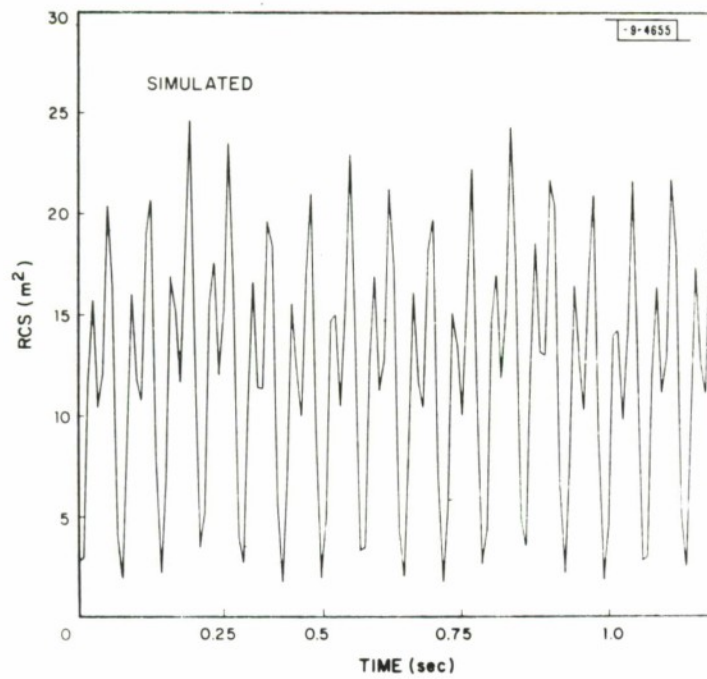


Fig. 16 Two cycles of ATS-3 signature at Arecibo. Comparison of simulated and measured results.

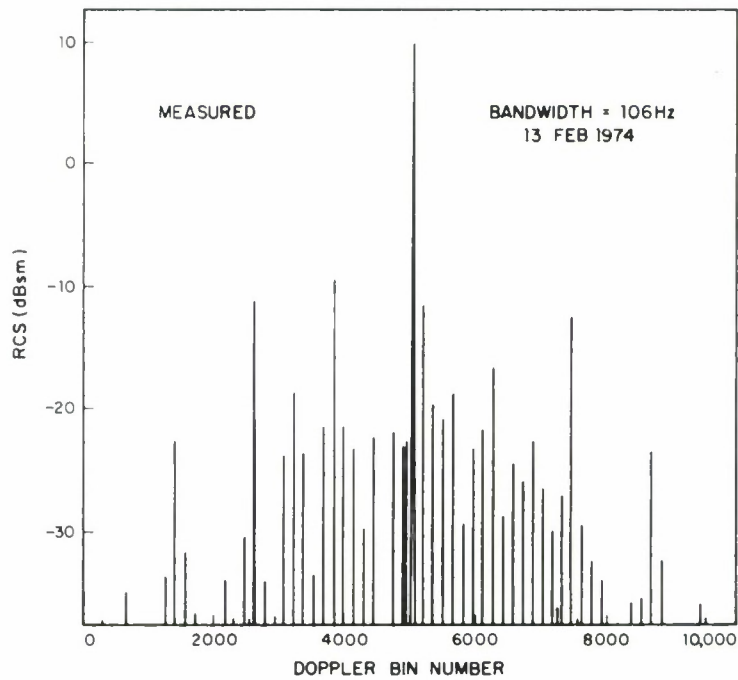
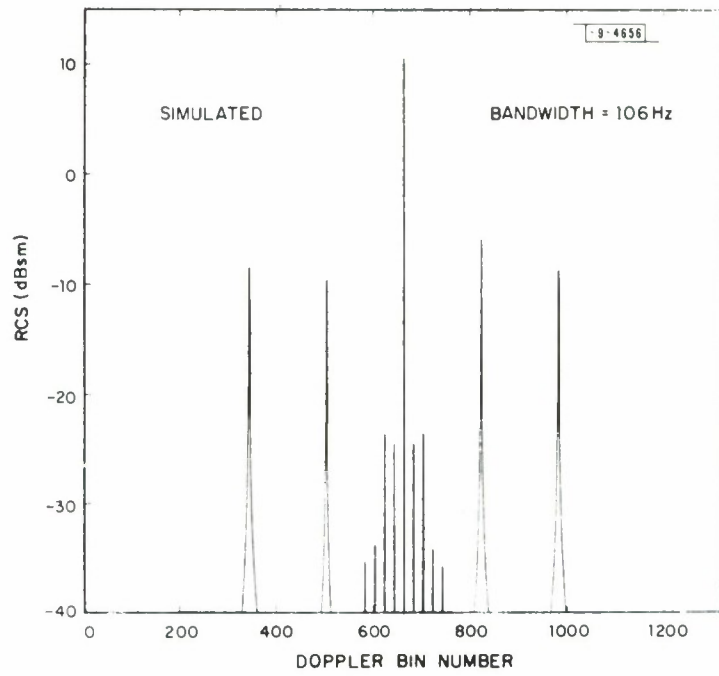


Fig. 17 Comparison of simulated and measured spectra of ATS-3 from Arecibo.

subsequent peaks, thereby giving the visual appearance of a reversal of time when comparing one trace to the other.

The major deficiency of the model is the way the parabolic antenna is treated. If it were better, undoubtedly the modeled time signature would be more in line with the measured one. Examination of the spectra of the actual and modeled signatures suggests the lobe widths of the actual antenna are narrower than predicted by the model. This could be verified by range measurements should the situation warrant it.

B. Millstone

The manner of modeling the scatters was qualitatively the same for L-Band as it was for UHF. An important quantitative difference was that due to the shorter L-Band wavelength the variation of the scattering properties with aspect angle is no longer negligible. The expected variation of peak cross section with aspect angle is shown in Figure 18. The plot was derived using the same qualitative models as for Arecibo: perfectly conducting body cylinder; unloaded wires for top T&C and bottom VHF antennas, and a set of flat plates for the parabolic cylindrical antenna. The considerations that were used to justify these models at Arecibo pertained at this frequency only a factor of three removed.

The simulated spectrum derived using the combined models is shown in Figure 19. It was computed for an aspect of 7° . By working with individual scatterers as inputs to the dynamic simulation, the following features of the spectrum were verified. First, the central spike is due almost entirely to the body cylinder. The spikes on either side of it are at harmonics of the spin frequency and out to the ninth harmonic are due mainly to the parabolic cylindrical antenna on the top of the spacecraft. The remaining spikes are from the top and bottom whip antennas.

A precise association of the spikes with the particular dipoles was not pursued since at best the results were near the noise level of the measured data. Note the mean noise level from data taken on 7 June 1974 shown on Figure 19.

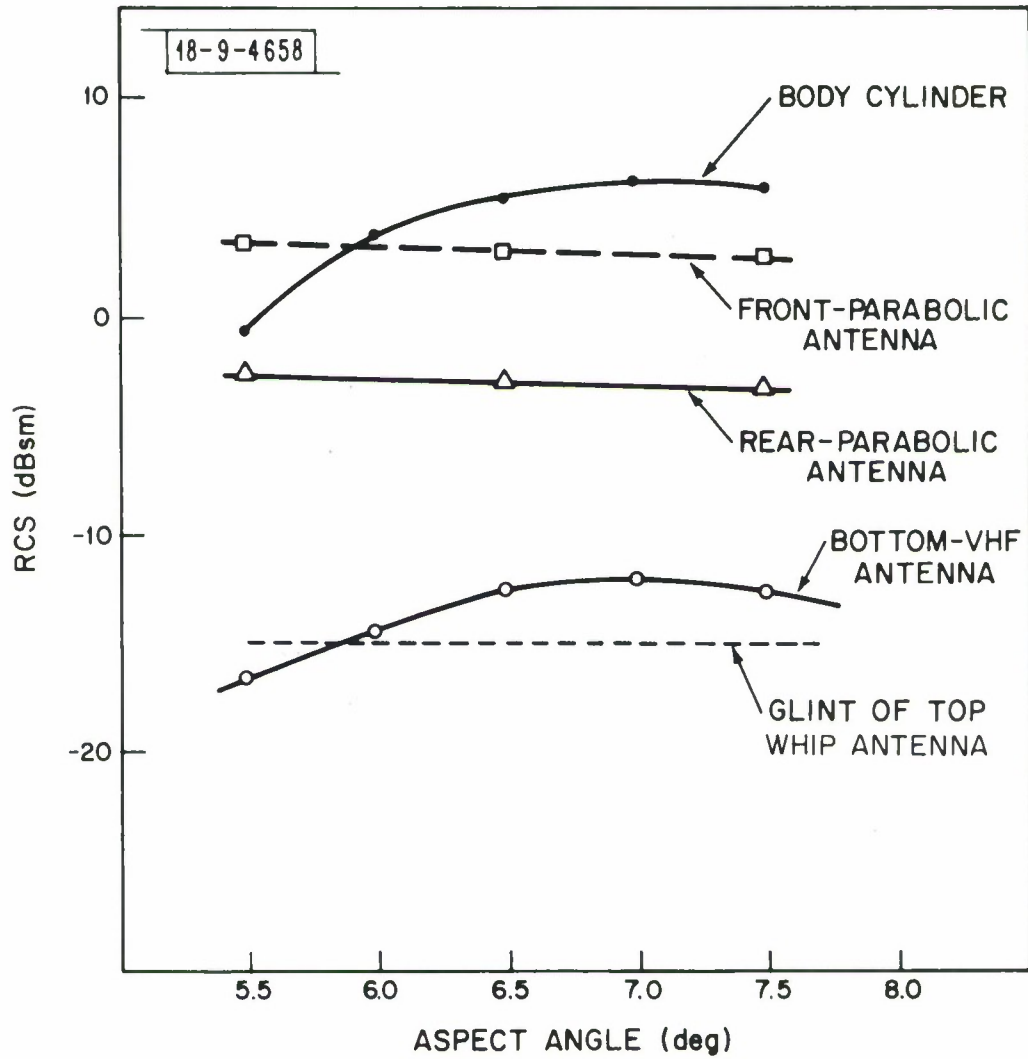


Fig. 18 Expected variation of peak RCS with aspect angle--Millstone radar.

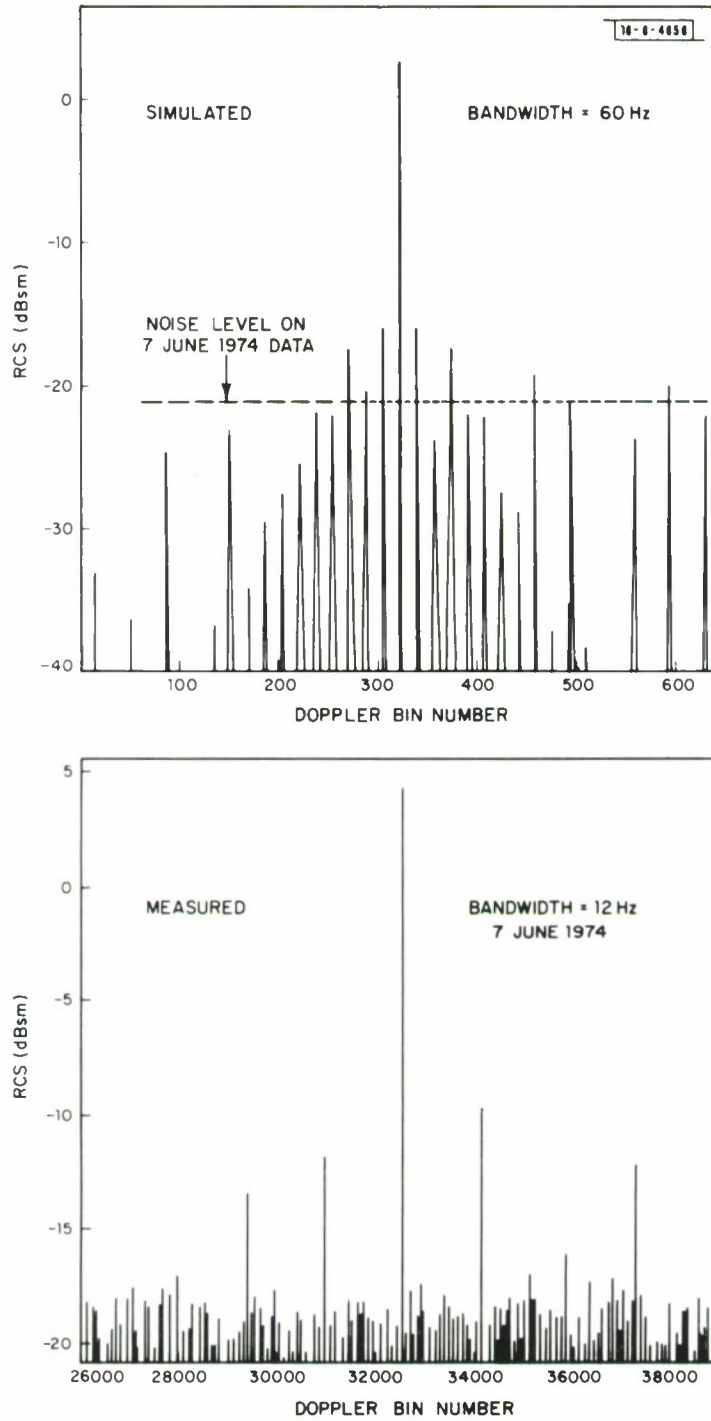


Fig. 19 Comparison of simulated and measured spectra of ATS-3 from Millstone.

The calculated result compares very well with the spectrum computed from data taken on 7 June 1974. The comparison is hampered only by the lack of sensitivity in the measured data (1000 sec. of coherent data were used in computing the spectrum; this represents the limit to coherent processing given by the frequency detent in the radar oscillator). Spikes that associate well with those calculated for the parabolic cylindrical antenna are readily apparent.

C. Haystack

The data taken at X-Band showed significant variation with aspect angle as would be expected from the scatterers being large compared to the wavelength. Figure 20 shows the expected variation in peak cross section with aspect angle for the major scatters.

As modeled the parabolic cylindrical antenna is the major scatterer at X-Band. The flat plate model resulted in null to null lobe widths of 19° for the front section and 31° for each of the rear sections. Typical variation of modeled cross section over the spin period is shown in Figure 21. The predicted spectrum of this scatterer is shown in Figure 22. The scattering lobe in the plane of the spin axis is sufficiently wide that these results are close to the same over the range of aspect angles we observed. Agreement between the magnitude of this spectrum with that measured, is excellent. It will be noted, however, the major lines in the modeled spectrum are spaced by twice the spin frequency, unlike the single spaced lines in the data. The likely explanation is the back of the antenna has been modeled as too strong and requires a more complex model than the flat plate one. A model accounting for true structure, including the holes seen in Figure 1 should give still better agreement.

From the perfectly conducting cylinder model used for the body cylinder, it would be expected to be the next strongest scatterer at many aspect angles. Furthermore, its contribution to the spectrum should be very significant and confined to a

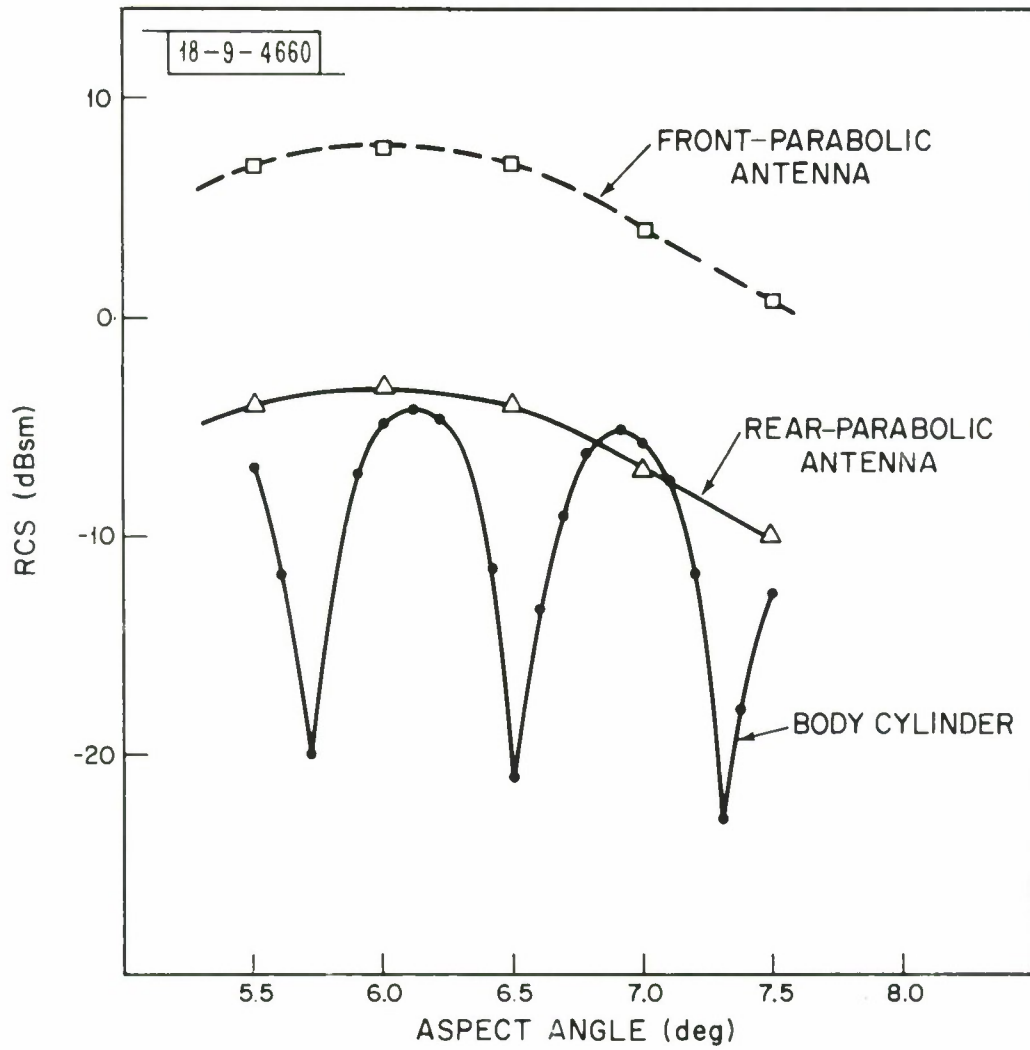


Fig. 20 Expected variation of peak RCS with aspect angle--Haystack radar.

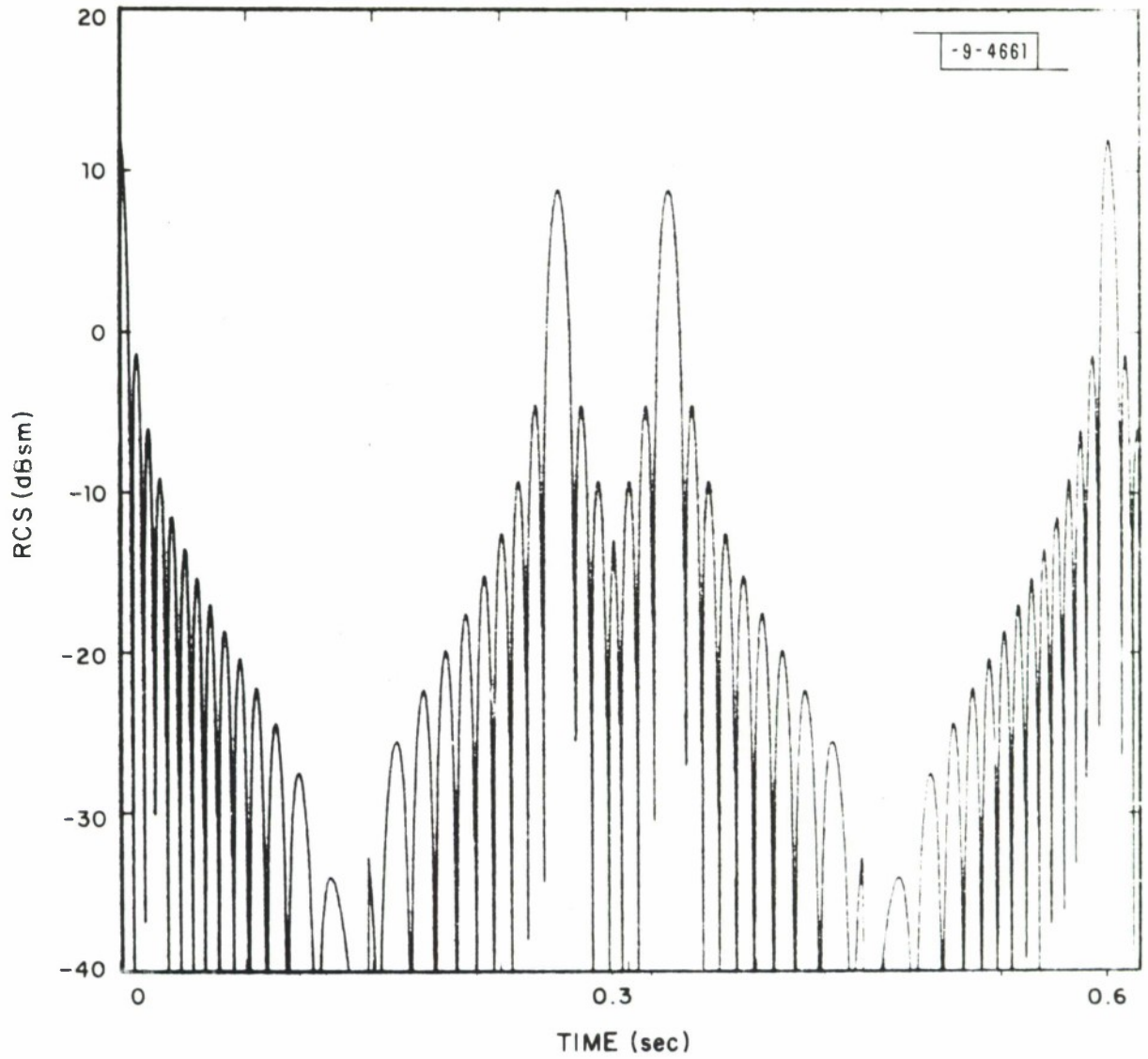


Fig. 21 Single cycle of ATS-3 parabolic cylindrical antenna signature at Haystack. Simulated result.

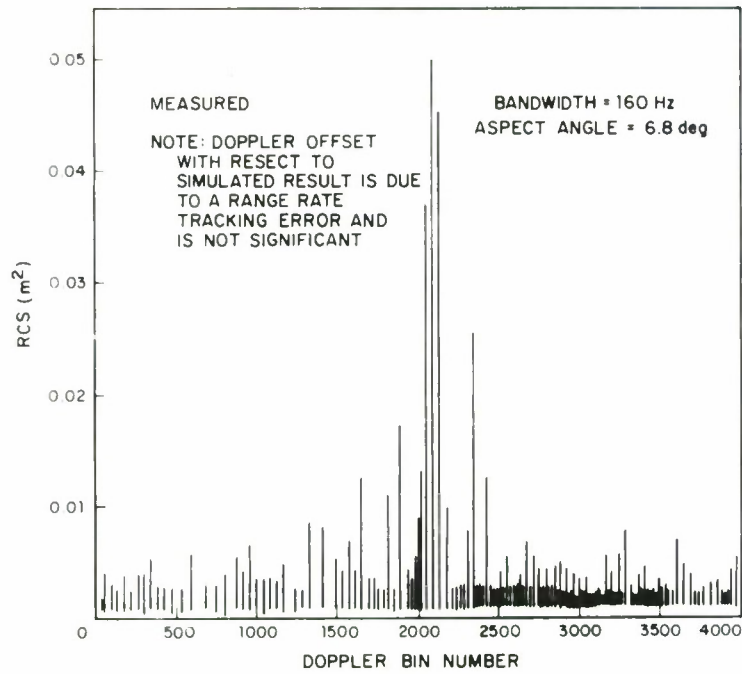
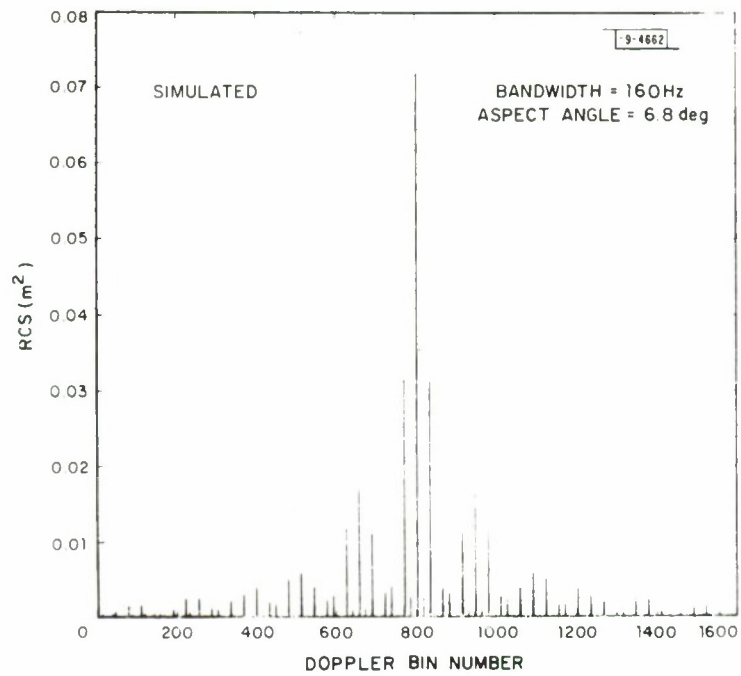


Fig. 22 Comparison of simulated spectrum of parabolic cylindrical antenna with measured spectrum of ATS-3 from Haystack .

narrow spike. In no case, however, was a spectral line identified that could be associated unambiguously with the body cylinder. In some instances, the most likely line was at least 10 dB below the calculated value.

The cause of this discrepancy appears due to the solar cell construction. The same behavior has been observed with ATS-1 and the Intelsat II series all of which have similar solar cells mounted on flat panels around the body (i. e., the body profile is a polygon not a circle). That such behavior is seen only at X-Band is most likely either a consequence of the departure from circularity or loading effects due to cell interconnection being negligible below this frequency.

As occurred at L-Band the dipoles contribution is sufficiently close to the noise level that it is not possible to make a definite association of observed and calculated behavior. The calculated spectrum for the dipoles shows the energy spread among a number of lines with all lines below -25 dBsm.

Comparison of the spectrum of the parabola alone, Figure 22, with the data, Figures 10-12, leads to the conclusion the parabolic cylinder is the major scatterer. Its model accounts well for both the spacing and strength of the spectral lines.

Despite the very low individual pulse returns encountered at Haystack, an attempt was made to produce a time signature by noncoherently adding a large number of cycles of data. Figure 23 shows the result of summing 800 sets of returns each of two satellite spin cycles duration. This represents about 1000 sec. of radar data. The figure makes clear that a periodic return does exist, but it is not possible to say much more. The long average has the undesirable effect of smearing out lobe widths and overall amplitude variations. Still the result is consistent with the notion of the major scatterer being the parabolic cylindrical antenna which glints periodically.

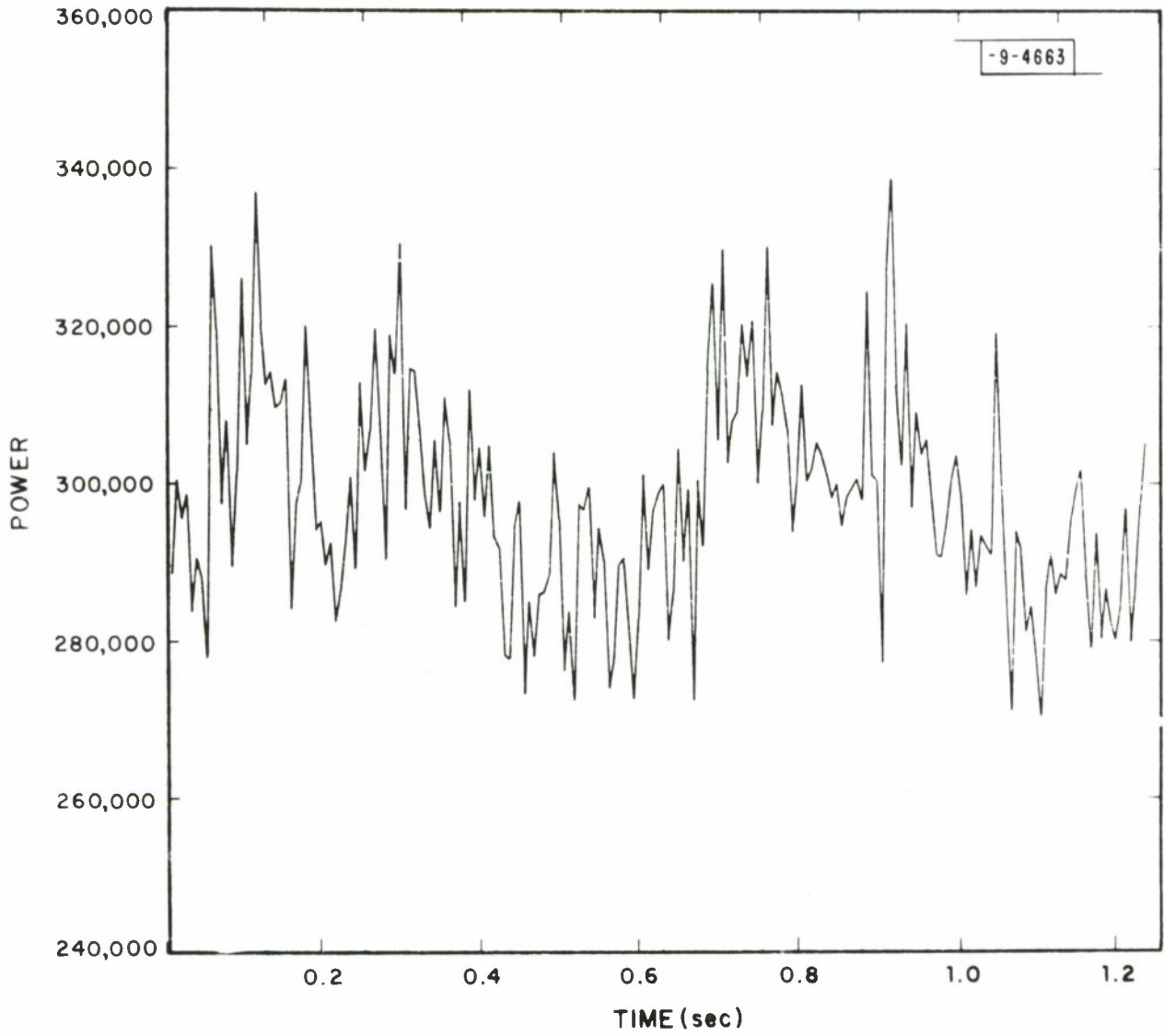


Fig. 23 Long noncoherent average of ATS-3 data from Haystack .

IV. COMPOSITE RESULTS

Table 7 summarizes the comparison of model predictions with observed behavior of the scatterers at the three radars. Agreement of the two is generally excellent apart from uncertainty about the behavior of the body cylinder as observed at X-Band. As noted this effect is most likely due to construction practices peculiar to a small class of satellites.

A feature of the three frequency observations of this target that becomes readily apparent in examining the table is that some scatterers can be seen at one frequency but not another. For example, while at X-Band the dipoles were not seen in a significant way, they make a major contribution to the UHF return. One can readily imagine other satellites and variations in aspect angle for which the situation would be reversed. The point of which is simple: while stabilized satellites often present little in the way of aspect angle variation to the observer, the use of several frequencies can effectively increase the number of features of the target that can be observed. This fact is a restrictive case of the practice of using multiple frequencies along with aspect angle variation to infer size and shape. Yet, it represents a means of doing diagnostic work on satellites which are stable, hence likely to be working and important.

While the inverse problem of inferring structure from returned power is far from being solved; it should be noted the signatures we have derived are sufficient at least to allow groupings of satellites based on characteristics like spin period, target stability and target amplitude.

TABLE 7

MODEL PREDICTIONS VS. OBSERVED BEHAVIOR

	430 MHz (ARECIBO)	1295 MHz (MILLSTONE)	7840 MHz (HAYSTACK)
Body Cylinder	Good agreement in RCS with theoretical value.	Good agreement in RCS with theoretical value.	Identification of spectral component ambiguous. Measured RCS at least 5-10 dB below theoretical.
Parabolic Cylinder	Model fits first few terms of spectrum well. Fails to account for higher harmonics	Model fits spectral components above noise level well.	Model fits major spectral components well and is consistent with highly averaged time signature.
Top Dipoles	Spectral components of dipoles accurately characterized by model. Dipoles account for major portions of time signature	Too small to allow meaningful statement.	Too small to allow meaningful statement.
Bottom Dipoles			

V. SUMMARY

Repeated observations of synchronous satellites from several radars have clearly demonstrated that detailed radar signatures of synchronous satellites can be obtained.

In the course of these observations a number of coherent processing techniques have been developed. Coherent integration times up to 1000 seconds have been utilized to improve on single pulse sensitivity by at least 40 dB at each radar.

From the analysis of observations of ATS-3 at UHF, L-Band and X-Band, it has been possible to identify and model the scattering behavior of the satellite with substantial agreement between model results and measured data.

ACKNOWLEDGMENT

The contributions of Thomas E. Clark who participated in data collection and whose programming efforts made much of the data collection and reduction possible and Antonio F. Pensa who participated in data collection are gratefully acknowledged.

REPORT DOCUMENTATION PAGE		READ INSTRUCTIONS BEFORE COMPLETING FORM
1. REPORT NUMBER ESD-TR-75-212	2. GOVT ACCESSION NO.	3. RECIPIENT'S CATALOG NUMBER
4. TITLE (and Subtitle) - Observations of Synchronous Satellite ATS-3 with Three Coherent Radars		5. TYPE OF REPORT & PERIOD COVERED Technical Note
		6. PERFORMING ORG. REPORT NUMBER Technical Note 1975-36
7. AUTHOR(s) Spence, Lee B. and Banner, Gerald P.		8. CONTRACT OR GRANT NUMBER(s) F19628-73-C-0002
9. PERFORMING ORGANIZATION NAME AND ADDRESS Lincoln Laboratory, M.I.T. P.O. Box 73 Lexington, MA 02173		10. PROGRAM ELEMENT, PROJECT, TASK AREA & WORK UNIT NUMBERS Project No. 2029 Program Element No. 63431F
11. CONTROLLING OFFICE NAME AND ADDRESS Air Force Systems Command Andrews AFB Washington, DC 20331		12. REPORT DATE 9 June 1975
		13. NUMBER OF PAGES 54
14. MONITORING AGENCY NAME & ADDRESS (if different from Controlling Office) Electronic Systems Division Hanscom AFB Bedford, MA 01731		15. SECURITY CLASS. (of this report) Unclassified
		15a. DECLASSIFICATION DOWNGRADING SCHEDULE
16. DISTRIBUTION STATEMENT (of this Report) Approved for public release; distribution unlimited.		
17. DISTRIBUTION STATEMENT (of the abstract entered in Block 20, if different from Report)		
18. SUPPLEMENTARY NOTES None		
19. KEY WORDS (Continue on reverse side if necessary and identify by block number) ATS-3 coherent processing RCS modeling synchronous satellite signatures		
20. ABSTRACT (Continue on reverse side if necessary and identify by block number) A series of observations of NASA satellite ATS-3 have been made using coherent UHF, L-Band and X-Band radars, and detailed signatures of the satellite have been obtained. Coherent processing techniques were implemented that increased each radar's sensitivity by at least 40 dB over single pulse performance. A scattering model has been developed that agrees substantially with the measured signature.		